공학박사 학위논문

물 직접분사 방법을 이용한 고분자 전해질막 연료전지의 공기극 가습 및 증발냉각에 관한 연구

Cathode humidification and evaporative cooling of Polymer Electrolyte Membrane fuel cells using direct water injection method

2016년 2월

서울대학교 대학원

기계항공공학부

황 성 훈

Abstract

Cathode humidification and evaporative cooling of Polymer Electrolyte Membrane fuel cells using direct water injection method

Seong Hoon Hwang
Department of Mechanical and Aerospace Engineering
The Graduate School
Seoul National University

Humidification and cooling are critical issues in enhancing the efficiency and durability of polymer electrolyte membrane fuel cells (PEMFCs). However, existing humidifiers and cooling systems have the disadvantage that they must be quite large to achieve adequate PEMFC performance. In this study, to eliminate the need for a bulky humidifier and to lighten the cooling load of PEMFCs, a cathode humidification and evaporative cooling system using an external-mixing air-assist atomizer was developed and its performance was investigated. The atomization performance of the nozzle

was analyzed experimentally under various operating conditions with minimal changes in the system design. Experiments with a five-cell PEMFC stack with an active area of 250 cm^2 were carried out to analyze the effects of various parameters (such as the operating temperature, current density, and water injection flow rate) on the evaporation of injected water for humidification and cooling performances. The experimental results demonstrate that the direct water injection method proposed in this study is quite effective in cathode humidification and stack cooling in PEM fuel cells at high current densities. The stack performance improved by humidification effect and the coolant temperature at the stack outlet decreased by evaporative cooling effect.

Keywords: Polymer Electrolyte Membrane Fuel Cell, Cathode Humidification, Evaporative Cooling, Direct Water Injection, External-mixing Air-assist Atomizer

***Identification Number*: 2009-23918**

Contents

List of Figures

List of Tables

Nomenclature

A	cross section area of the duct [m^2]
A_s	surface area of drop [m^2]
C_d	coefficient of drag
C_p	specific heat of air [J/kg·℃]
D	drop diameter [m]
g	constant for gravity [m/s^2]
h	heat transfer coefficient [$W/m^2 \cdot ℃$]
h_a	enthalpy of air [J/kg]
h_d	enthalpy of drop [J/kg]
h_{fg}	enthalpy of evaporation [J/kg]
$h_{fg,wall}$	enthalpy of evaporation at duct wall temperature [J/kg]
h_m	mass transfer coefficient
$h_{m,wall}$	mass transfer coefficient of duct wall
h_{wall}	heat transfer coefficient of duct wall
k_a	thermal conductivity of air [W/m·℃]
L	duct length [m]
n	number of drops per second per unit cross section area of the duct
Nu	Nusselt number
P	duct perimeter [m]

Pr	Prandtl number
Re_d	drop Reynolds number
Sc	Schmidt number
Sh	Sherwood number
T_a	air temperature [℃]
T_d	drop temperature [℃]
T	water temperature [℃]
T_{wall}	temperature of duct wall surface [℃]
U_x	drop velocity in x-direction [m/s]
U_y	drop velocity in y-direction [m/s]
u	air velocity [m/s]
W	relative velocity of drop, air
We	Weber number of drop
X	mass fraction of water vapor
X_s	mass fraction of water vapor at the drop surface
X_{wall}	mass fraction of water vapor at the surface of duct wall

Greek symbol

σ	surface tension [N/m]
ρ_a	density of air [kg/m^3]
ρ_l	density of water [kg/m^3]
μ_a	absolute viscosity of air [Pa·s]

λ	ratio of air to vapor molecular weight
ω	humidity ratio
ν_a	kinetic viscosity of air [m^2/s]

Subscripts

a	air
d	drop
fg	evaporation
l	liquid condition
m	mass transfer condition
s	surface, saturation condition
v	vapor
wall	duct wall condition
x	coordinate
y	coordinate

Chapter 1. Introduction

1.1 Background of the study

Energy is an essential driving force for modern society. In particular, electricity has become standard source of power for almost every aspect of life. However, it has become apparent that the current methods of producing this most valuable commodity, combustion of fossil fuels, are of limited supply and have become detrimental for the earth's environment. For these reasons, much effort is now being placed on eliminating the use of combustion of non-renewable fuels as a source of power. One of the most promising alternatives to the fossil fuel in the production of electric power is the hydrogen fuel cell. Especially, PEM (polymer electrolyte membrane) fuel cells are regarded suitable for vehicle power applications. The PEM fuel cell has many advantages over the current internal combustion engine. It can achieve much higher efficiencies than a combustion cycle. The PEM fuel cell is also environmentally friendly. Other advantages of this fuel cell system include simplicity of design, low noise operation and economic independence.

Most of polymer electrolyte membranes of PEM fuel cells must be humidified to maintain high ion conductivity for electrochemical reaction. In

addition to this, appropriate humidification protects membranes from the damage caused by the heat generation in PEM fuel cells. For this reason, PEM fuel cell systems need a large amount of water for humidification. As it is not desirable for users to replenish de-ionized water, water produced in the fuel cell stack is usually recycled for humidification. For example, in an automotive PEM fuel cell system, a large amount of water is exhausted as vapor from the outlet port of the fuel cell stack. This moist is usually trapped in water reservoir through heat exchangers like condensers, or directly supplied to humidifiers like a gas-to-gas membrane humidifiers. However, existing humidifiers have the disadvantage that they must be quite large to achieve adequate PEMFC performance and it is a barrier to miniaturize fuel cell systems.

Water management is directly linked with heat management. When heat removal from the stack is not sufficient, heat balance of the system will be broken and this will cause temperature rising of the stack which may cause overheat damage of the PEM fuel cell stack. Moreover, as the stack temperature rises, massive amount of water will be vaporized and exhausted away, which may break water balance of the PEM fuel cell system. Thus, it is necessary to investigate the novel method for both humidification and heat removal.

1.2 Literature survey

In a PEMFC, in which a polymer membrane (typically perfluorosulfonic acid, PFSA; Nafion®) is used as an electrolyte, humidification is required to achieve good performance because the ion conductivity of the PFSA membrane is determined by its water content. Therefore, humidification is one of the important operating conditions directly affecting fuel cell performance. As shown in Table 1.1, there are various methods of humidification for PEM fuel cell systems and each kind of methods has advantages and drawbacks. Humidification methods can be categorized as internal or external type according to the place of humidifier. Among them, Membrane type is the most widely used humidifier for automobiles because it has high performance and self-regulating characteristics together with small consumption of energy (Fig. 1.1(a)). The hot and humid exit air passes small membrane tubes and the cool and dry inlet air flows outside of the tubes. Water vapor diffuses to membrane from damp outlet air to dry inlet air by partial pressure difference. By this process, temperature of inlet air increases and can have the potential to contain more moist. This type humidifiers use thousands of membrane tubes which is the same type used as the membrane in the PEM fuel cell. Normally Nafion® is used for the tubes and this is expensive and the durability is not so high. Moreover big pressure drop happens when exit air passing the

Table 1.1 Humidification methods for PEM fuel cells

Types	Internal or External	Positive factor	Negative factor	Reference
Self humidification	Internal	Simple	Difficult to control	Buchi and Srinivasn (1997)
Porous bipolar plates	Internal	Simple	Expensive	Staschewski (1996)
Absorbent wick	Internal	Simple	Difficult to control	Shanhai Ge et al. (2004)
Metal foam	Internal	Simple	Metal corrosion	Floyd (2001)
Bubbling	External	High dew point	Need much heat	
Steam injection	External	Easy to control	Need much heat	
Membrane (liquid-to-gas)	External	Simple Energy saving	Expensive, Low durability Leakage possibility, Bulky	Chow et al. (1998)
Membrane (gas-to-gas)	External	Simple Energy saving	Expensive, Low durability Bulky	Paul Scherrer Institue (1999)
Enthalpy wheel	External	Compact	Preheated reactant gases	
Direct water injection	External	High durability Easy to control	Complicated apparatus Need water tank	Wood et al. (1998)

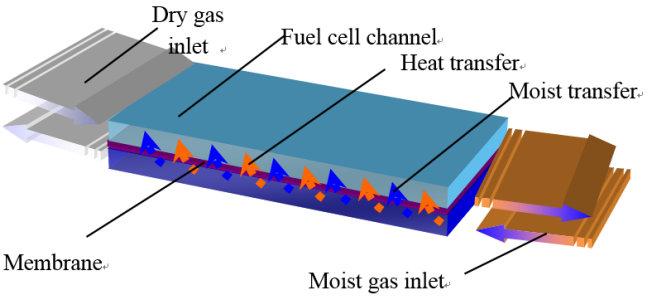

(a) Membrane humidification (gas-to-gas)

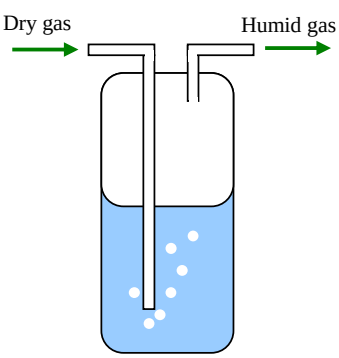

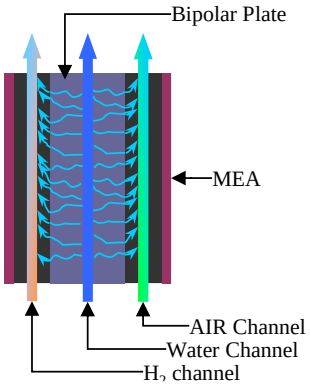

(b) Bubbling humidification (c) Porous carbon foam humidification

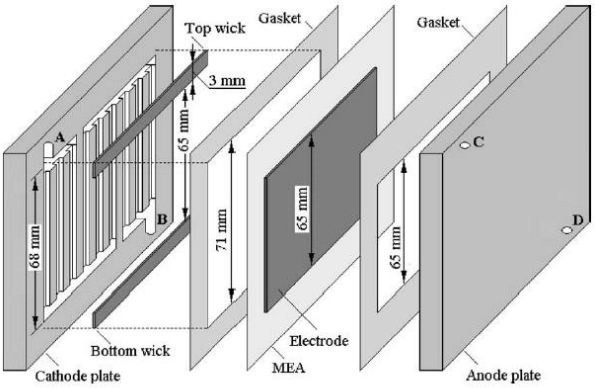

Fig. 1. Schematic of the cell structure with two strips of absorbent wicks.

(d) Absorbent wick

Figure 1.1 Schematic diagrams of various humidification type

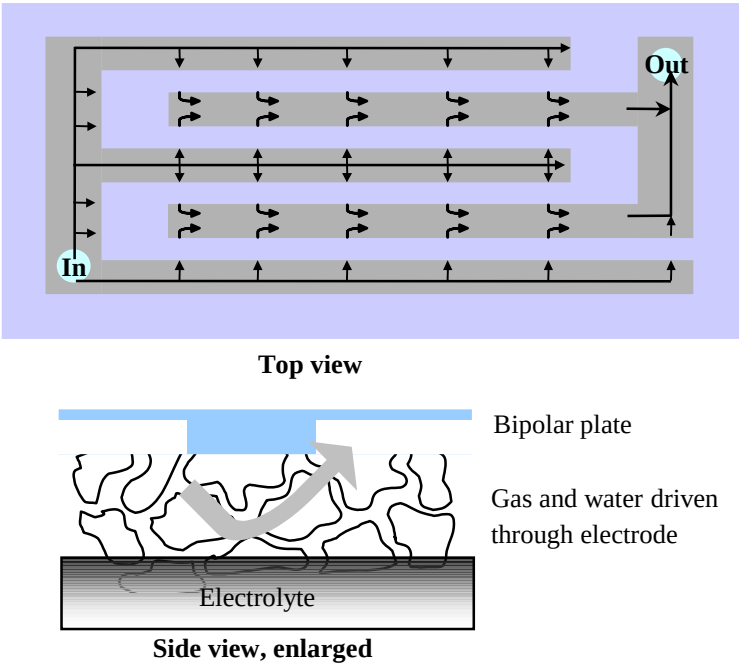

(e) Direct water injection with inter digitized flow channels

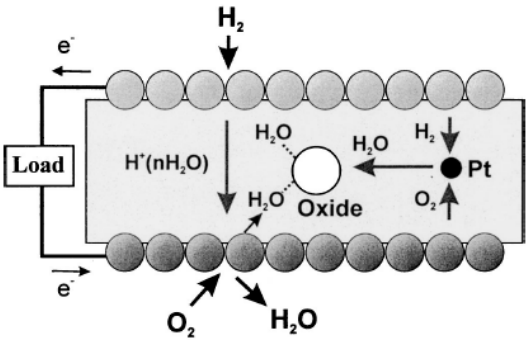

(f) Self humidifying electrode membrane

Figure 1.1 Schematic diagrams of various humidification type

small tubes.

Fig. 1.1(b) shows schematic of bubbling type humidifier which is commonly used in laboratory test systems. The reactant gases of fuel cells are humidified by passing through the water whose temperature is controlled. This is good for experimental work, but not applicable to automobiles because of large energy consumption.

Humidification using porous bipolar plate is internal humidification type and it was proposed by Staschewski. In this type, water is supplied to membrane from cooling water channel through small pores which formed in the bipolar plate (Fig. 1.1(c)).

Fig. 1.1(d) shows the schematic view of absorbent wick applied fuel cell. The sponges installed in the fuel cell absorb water from air outlet area and transport it to inlet area by capillary force. It is very simple, easy to manufacture and very cheap. Moreover, it does not cost power consumption. But it also has disadvantages such as the need of high pressure and difficulty of controlling. If these problems are solved, it can be a good solution as a humidifier for fuel cell vehicles.

Fig. 1.1(e) shows direct water injection type. It was invented by Wood et al. and the liquid water is injected directly to interdigitated flow field. Normally direct water injection to fuel cell leads to the electrode flooding.

However, interdigitated flow field makes reactant gases to blow the water through the cell and over the entire electrode. In this type the reactant gases must be pressurized to pass through the gas diffusion layer and high pressure costs much power consumption.

Other form of humidification is using a self humidifying electrolyte membrane. Generally membrane permeates only protons; hydrogen ions. However a small amount of hydrogen and oxygen crosses over the membrane. This causes voltage drop and fuel waste. The Pt nano-particles in self humidifying electrolyte membrane suppress crossover by catalytic recombination of crossover hydrogen and oxygen and the produced water gives moist to the membrane (Fig. 1.1 (f)). It has advantages of not having additional equipments, good performance and rapid start up at low temperature. However manufacturing process is complex and the price is expensive.

Likewise, heat rejection of PEMFCs has very important effects on their performance and durability. Although PEMFCs have very high energy conversion efficiency, they produce an amount of waste heat proportional to their electrical power output. Furthermore, a higher temperature can accelerate the degradation of the membrane and catalyst and reduce the stack performance. Thus, the heat generated should be removed effectively to avoid

overheating of the stack components, especially the membrane, and to maintain a favorable operating temperature range, which is usually from 60 to 80℃. Although many cooling methods are exist, to obtain sufficient cooling capacity that can manage a large amount of heat generated by PEMFC in high power region a very large heat transfer area is required. However, when stringent space requirements must be met, the radiator size must be limited, and cooling capacity is thus restricted. In such cases, the stack temperature may rise above 80℃, so its output power should be limited to prevent overheating of the stack, especially under harsh heat rejection conditions, such as operation in summer. Given these challenges, a novel technique for humidification and cooling of PEMFCs is greatly needed.

Studies of systems for both humidification and evaporative cooling by water injection have been conducted. However, it is difficult to identify practical applications or study dealing with both humidification and evaporative cooling issues at the same time. Furthermore, some of these systems require changes to the stack design or use of supplementary devices that consume electrical power or increase the manufacturing cost and system complexity.

For commercialization of fuel cell vehicles, humidifiers must meet both high humidification performance and low energy consumption for

humidification. Moreover, it is necessary to have high durability, low cost for manufacturing and compact size. And proper heat management is also required.

1.3 Objectives and scopes

In this study, to eliminate the need for a bulky humidifier and to lighten the cooling load of PEM fuel cells, a cathode humidification and evaporative cooling system using an atomizer was developed and its performance was investigated both numerically and experimentally.

In chapter two, numerical simulation of humidification performance using atomizer is mainly discussed. In order to carry out this simulation, an atomizer suitable for PEM fuel cell systems was investigated and water evaporation in the cathode channel was modeled numerically. Finally, from the result of the atomizer and the humidification model, PEM fuel cell performance was simulated.

In chapter three, a direct water injection system using an air-assist nozzle was developed and its feasibility test was conducted. Humidification and evaporative cooling performance was investigated experimentally with large area PEM fuel cell stack of 250 cm^2 especially focusing on the high current

region which require large amount of humidification and cooling loads.

In chapter four, the operating characteristics of PEM fuel cells with a direct water injection system were investigated to provide useful information and better understanding on this system. Water injection flow rate, water injection temperature, stack operating temperature, stack operating pressure and cathode stoichiometric ratio are considered as operating variables. An operating strategy applying intermittent water injection and the effect of water injection on start-up process also investigated.

In chapter five, conclusions are given along with the brief summarization

Chapter 2. Numerical analysis on the cathode humidification of direct water injection method

2.1 Introduction

There are various methods of humidification for PEM fuel cell, and each kind of humidifiers has advantages and drawbacks. Among them, membrane humidification is commonly used to PEM fuel cell. There are two types of membrane humidification, liquid-to-gas method and gas-to-gas method. Chow et al. (1998) have reported a membrane humidification which is type of liquid-to-gas method. Hydrogen and oxidant gases are humidified by passing the gas on one side of the membrane and deionized water on the other side before entering the fuel cell. In such arrangements, deionized water is transferred across the membranes to the fuel and oxidant gases like air. This kind of humidifiers is usually based on the planar structure similar to PEM fuel cell stacks except gas diffusion layer, but apparatus itself is too expensive and durability of humidifier is low. In 1999, Paul Scherrer Institute proposed gas-to-gas type membrane humidifier which uses hot and humid exhaust gas to humidify dry incoming gas through membranes. Generally, this gas-to-gas membrane humidifiers have numerous tubular bundles made of Nafion®

membranes which is shown in Fig. 1.1. This kind of humidifiers can simplify the water management system, because they use the moist contained in exhaust gas. Moreover, membrane humidifier also can be operated as heat exchanger. So it is possible to humidify gases at temperatures close to the operating temperature of the fuel cell. However, it is difficult to control the humidity and it is not sufficient in high power range of the system. Besides, due to its massive volume PEM fuel cell systems become larger and this is negative factor in commercialization. This is why novel method for humidification of PEM fuel cells which have compact size is required.

2.2 Numerical model of cathode humidification

2.2.1 Selection of atomizer and its model

Injector is fluidic device which can provide a liquid jet by pressurizing a liquid or gas thorough small nozzles. Atomizer is a kind of injector for the purpose of transforming the bulk liquid into droplet. The process of atomization is one in which a liquid jet or sheet is disintegrated by the kinetic energy of the liquid itself, or by exposure to high-velocity air or gas. As their name suggests, pressure atomizers rely on the conversion of pressure in

kinetic energy to achieve a high relative velocity between the liquid and the surrounding gas (see Fig. 2.1 (a)). They include plain-orifice and simplex nozzles, as well as various wide-range designs such as variable-geometry, duplex, and dual-orifice injectors (see Table 2.1). Air-assist atomizers use the beneficial effect of flowing air in assisting the disintegration of a liquid jet or sheet (see Fig. 2.1 (c)). It is operated at low injection pressure with air or steam. In principle, the airblast atomizer functions in exactly the same manner as the air assist atomizer (see Table 2.1). The main difference between the two systems lies in the quantity of air employed and its atomizing velocity. Air velocity through an airblast atomizer is limited to a maximum value (usually around 120 m/s), and a large amount of air relative to supplying liquid is required to achieve good atomization.

This study is based on air-assist type injectors. To facilitate evaporation of injected water in the cathode channel, it is important to atomize liquid water into very fine droplets because heat and mass transfer rates increase as the droplet size decreases and the total surface area increases. Taking into consideration this principle and the characteristics of a PEMFC system, particularly the air-providing part, we selected an external-mixing air-assist nozzle as the atomizer. This atomizer produces the finest droplets possible for a given liquid flow rate and air supplying pressure. In contrast to single-fluid

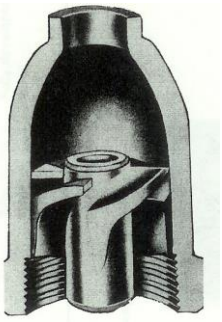

(a) Solid cone simplex nozzle (Courtesy of Delavan, Inc.)

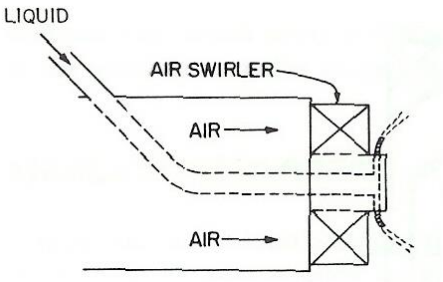

(b) Plain-jet airblast atomizer (Jasuja)

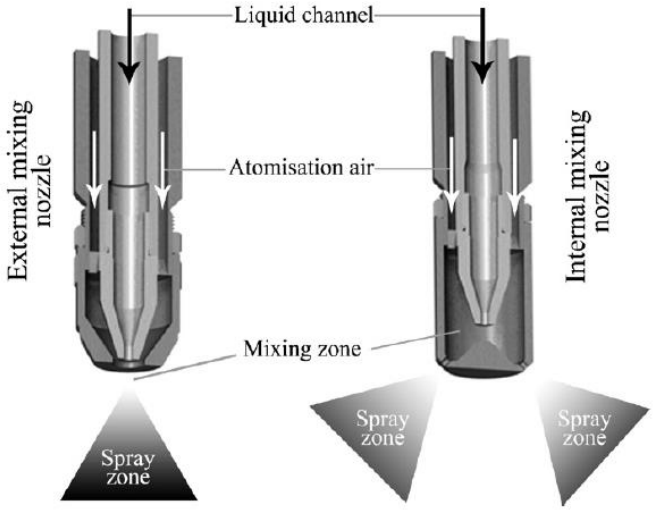

(c) Air assist nozzle (Salman et al., 2007)

Figure 2.1 Various injectors for atomization

Table 2.1 Positive and negative factors of various types of atomizers

Types	Description	Positive factor	Negative factor
Pressure atomizer	Plain orifice	Simple, Cheap	Narrow spray angle
	Simplex	Simple, Cheap Wide spray angle	Needs high supply pressure
	Duplex	Simple, Cheap Wide spray angle	Spray angle narrow as liquid flow rate is increased
Air-assist	Internal mixing	Good atomization Prevent clogging Can atomize high viscosity liquids	Liquid can back up air line Needs external source of high pressure air or stream
	External mixing	Good atomization Prevent clogging Can atomize high viscosity liquids	Needs external source of high pressure air or stream Does not permit high AFR ratio
Air blast	Plain jet	Easy to control	Narrow spray angle Atomizing performance inferior to prefilming airblast
	Prefilming	Good atomization at high air pressure Wide spray angle	Atomization poor at low air velocities

atomizers that require high pressures to produce fine sprays, air-assist atomizers can produce fine sprays at relatively low pressures such as 50 kPa of pressure difference at minimum. This atomizers also have several other advantages over internal mixing-type atomizers, including ease of control, fine atomization performance with high uniformity, and low likelihoods of malfunctioning, and erosion. Furthermore, the liquid may be introduced either under pressure or without excess pressure using an external-mixing air-assist atomizer. Accordingly, without a pump, the nozzle is able to atomize and discharge liquid water using just a high-velocity air stream. Although this type of nozzle requires a high air-to-liquid ratio (ALR) in terms of the mass flow rate ($\mathrm{ALR} = \dot{m}_{\mathrm{air}} / \dot{m}_{\mathrm{liq}}$), PEMFC systems have air-providing devices such as blower or compressor that can accommodate high air flow rates.

The nozzle specifications were based on the range of air flow rates of a five-cell PEMFC stack with an active area of 250 cm^2. Assuming that the water required for injection is supplied from the water produced in the PEMFC, the water production rate of the stack was also considered. The mass flow rate of the cathode inlet air and the PEMFC water production rate are determined as follows.

$$\dot{m}_{\mathrm{air,\,in}} = \frac{I \cdot N \cdot M_{\mathrm{air}}}{4F \cdot x_{\mathrm{O_2}}} \cdot \lambda_{\mathrm{cathode}} \tag{2.1}$$

$$\dot{m}_{\text{water, product}} = \frac{I \cdot N \cdot M_{\text{water}}}{2F} \tag{2.2}$$

When the stoichiometric ratio (SR) and current density are 2.0 and 1.2 A/cm^2, respectively, which are typical values for general operating conditions at high current densities, the mass air flow rate and the water production rate are 1.075 g/s and 0.140 g/s, respectively. The spray should have a narrow angle and centralized pattern to avoid as much as possible the droplets impinging with the inner surface of the tubes, because the nozzle orifice is positioned in the air providing tubes of cathode inlet. Considering all of the above factors, we selected an external-mixing air-assist nozzle with a round spray pattern. Figure 2.2 shows a schematic illustration of the coaxial, external-mix air-assist nozzle (Spraying Systems Co., Chicago, Illinois, USA, SU1A setup) used in this study and its spray pattern. This nozzle requires an air flow rate of 17 l/min (= 0.341 g/s at 20℃, 1 bar) at 1.5 bar of air supplying pressure and has a spray angle of 18° with a round pattern. These characteristics are quite suitable, given the selection criteria stated above.

The spray droplet size is a crucial parameter of the atomization process. Because of the complex and random nature of the atomization process, the spray can be regarded as a spectrum of droplet sizes distributed around some

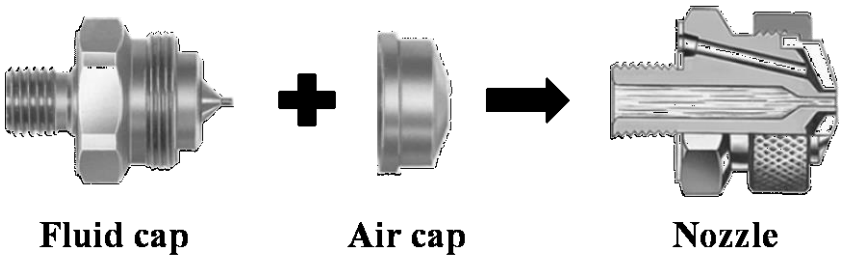

(a) schematic

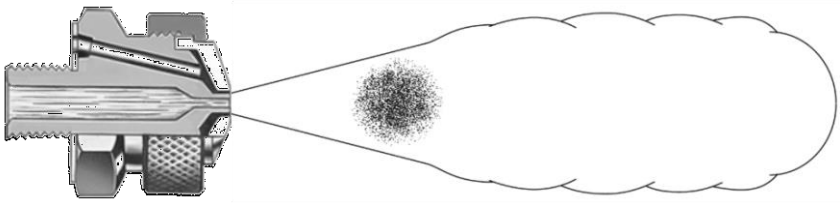

(b) round spray pattern

Figure 2.2 Coaxial external-mix air-assist nozzle

defined mean droplet size. At present, the most widely used mean diameter definition may be the Sauter mean diameter ($\mathrm{SMD} = D[3,2] = d_{32} = \sum n_i d_i^3 / \sum n_i d_i^2$, where n_i is the number of droplets per unit volume in size class i and d_i is the droplet diameter) for air-assist atomizer. Equation (2.3) is a semi-empirical droplet size correlation for water and aqueous solutions of glycerol derived by Walzel. According to Hede et al., Walzel's equation is the best choice for use in estimating the droplet size in atomized aqueous solutions, including water.

$$d_{32} = d_{\text{orifice}} \cdot 0.35 \cdot \left[\frac{\Delta P_{\text{air}} \cdot d_{\text{orifice}}}{\gamma_{\text{liq}} \cdot \left(1 + \frac{\dot{m}_{\text{liq}}}{\dot{m}_{\text{air}}}\right)^2} \right]^{-0.40} \cdot (1 + 2.5 \cdot \text{Oh}) \tag{2.3}$$

In this equation, d_{orifice} is the nozzle orifice diameter, ΔP_{air} is the pressure drop in the gas through the nozzle (often simplified as the difference between the nozzle pressure and the ambient pressure into which the nozzle stream expands), γ_{liq} is the liquid surface tension, and Oh is the Ohnesorge number that relates the viscous forces to the inertial and surface tension forces, according to Eq. (2.4).

$$\text{Oh} = \frac{\mu_{\text{liq}}}{\sqrt{\gamma_{\text{liq}} \rho_{\text{liq}} d_{\text{droplet}}}} \approx \frac{\text{viscous forces}}{\sqrt{\text{inertia} \cdot \text{surface tension}}} \tag{2.4}$$

In this equation, μ_{liq} is the dynamic viscosity of liquid and ρ_{liq} is the

liquid density. For liquids with low viscosity such as water, the Ohnesorge number rarely influences the droplet size as much as other parameters do. As mentioned previously, the ratio between $\dot{m}_{air}$ and $\dot{m}_{liq}$ is referred to as the ALR.

2.2.2 Humidification model of injected water

Figure 2.3 shows the humidification model and control volume for analysis. As the flow proceeds downstream, perfect transverse mixing is assumed at each location. Thus, heat and mass transfer from a drop in the control volume is assumed to spread immediately and uniformly everywhere in the control volume. The channel wall is assumed to be adiabatic, but heat and mass transfer due to evaporation from walls are included in the model. The duct pressure is assumed to be constant and equal to the ambient pressure as a result of which momentum transfer between drops and air is neglected.

To carry out humidification simulation, it is necessary to consider related governing equations. In this study, mass, momentum and energy conservation equations are considered. Drag coefficient flow around the droplet, mass concentration properties, heat and mass transfer correlations are also

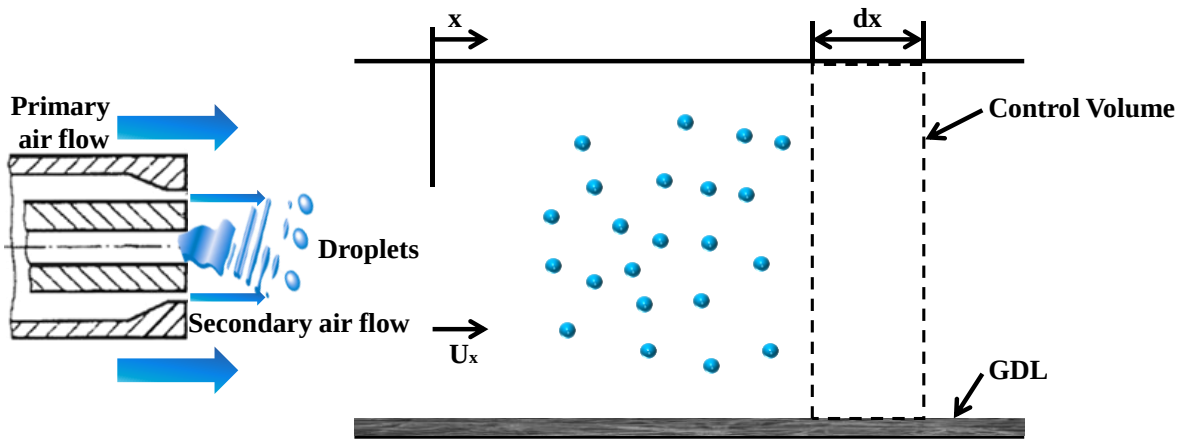

Figure 2.3 1-Dimensional model of droplet evaporation

considered.

Conservation of mass

The conservation of water vapor mass in air can be expressed as Eq. (2.5) where the increase in mass and mass fraction of water in the air water mixture (X) occurs due to evaporation of drops, channel surface.

$$\frac{dX}{dx} = \frac{n_d h_m A_s \left(X_s - X \right)}{U_x u} + \frac{h_{m,wall} P \cdot \left(X_{wall} - X \right)}{Au} - \frac{X}{u}\frac{du}{dx} - \frac{X}{\rho_a}\frac{d\rho_a}{dx} \tag{2.5}$$

The drop evaporation causes mass loss which is reflected in there decreasing diameters. The conservation of drop mass can be written as Eq. (2.6).

$$\frac{dD}{dx} = \frac{h_m \rho_a \left(X_s - X \right)}{\rho_l U_x} \tag{2.6}$$

Conservation of momentum

For air, the conservation of x-momentum represents the balance of air acceleration with momentum addition from drops, change of mass (due to evaporation from drops), pressure gradient in duct and wall shear stresses (Kachhwaha, 1996). In the model of this study, air pressure was assumed constant throughout the channel. Momentum assumed to be negligible and, therefore, the air momentum equation is not used in the simulations.

The deceleration of drops in x-direction can be expressed as Eq. (2.7).

$$\frac{dU_x}{dx} = -\frac{0.75 C_D \rho_a W (U_x - u)}{U_x \rho_l D} - \frac{3U_x}{D}\frac{dD}{dx} \tag{2.7}$$

Here, the right-hand side represents drag force and inertia force occurring due to drop mass change.

Conservation of energy

Change in air temperature occurs due to mass and heat transfer from droplets and from the channel walls which can be expressed as Eq. (2.8)

$$\begin{aligned}\frac{dT_a}{dx} &= \frac{\left[n h_{fg} \pi D^2 h_m \rho_a (X_s - X) - n h \pi D^2 (T_a - T_d) \right]}{C_{p,a} \rho_a u U_x} \\ &+ \left[h_{fg,wall} h_{m,wall} \rho_a (X_{wall} - X) - h_{wall} (T_a - T_{wall}) \right] \left[\frac{P}{C_{p,a} \rho_a u A} \right] \\ &- \frac{h_a}{C_{p,a}} \left[\frac{1}{u}\frac{du}{dx} + \frac{1}{\rho_a}\frac{d\rho_a}{dx} \right] - \frac{h_{fg}}{C_{p,a}}\frac{dX}{dx}\end{aligned} \tag{2.8}$$

Energy balance of drops represents the rate of change of drop temperature, and the mass and heat transfer occurring with air.

$$\frac{dT_d}{dx} = \frac{6\left[h(T_a - T_d) - h_{fg} h_m \rho_a (X_s - X) \right]}{D \rho_l U_x C_{p,d}} - \frac{3h_d}{C_{p,d} D}\frac{dD}{dx} \tag{2.9}$$

Drag coefficient

Here each drop is assumed to behave like a rigid sphere for which drag coefficient-Reynolds number relations are available (Lin et al., 1988).

$$
\begin{aligned}
&C_D = 24/\mathrm{Re}_d && for\ \mathrm{Re}_d < 2 \\
&C_D = 18.197/\mathrm{Re}_d^{0.599} && for\ 2 < \mathrm{Re}_d < 500 \\
&C_D = 0.44 && for\ 500 < \mathrm{Re}_d < 2\times 10^5
\end{aligned} \tag{2.10}
$$

Here, Re_d is the drop diameter Reynolds number based on velocity of drops relative to the air which is expressed as Eq. (2.11) and (2.12).

$$\mathrm{Re}_d = \frac{\rho_a W D}{\mu_a} \tag{2.11}$$

$$W = U_x - u \tag{2.12}$$

Mass concentration properties

The mass concentration of water vapor at the drop surface is given by Eq. (2.13).

$$X_s = \frac{p_{vs}}{\lambda p - (1-\lambda) p_{vs}} \tag{2.13}$$

where, λ is the ratio of the air to vapor molecular weight, p_{vs} the partial pressure of water vapor and p the total atmospheric pressure. For air water vapor mixture, λ is equal to 1.608. In general, p_{vs} can be approximated by the saturation pressure corresponding to the droplet temperature.

The mass fraction of water vapor in air can be expressed as Eq. (2.14).

$$X = \frac{\omega}{1+\omega} \tag{2.14}$$

where, ω is humidity ratio, which is related to the saturation pressure p_{vs}.

Heat and mass transfer correlations

The heat and mass transfer coefficients for droplets have been determined from the correlations developed by Ranz and Marshall (1952).

$$\mathrm{Sh} = \frac{h_m D}{\delta} = 2.0 + 0.6\,\mathrm{Re}_d^{\,0.5}\,\mathrm{Sc}^{0.33} \tag{2.15}$$

$$\mathrm{Nu} = \frac{hD}{k_a} = 2.0 + 0.6\,\mathrm{Re}_d^{\,0.5}\,\mathrm{Pr}^{0.33} \tag{2.16}$$

where, Sc is the Schmidt number and Pr is the Prandtl number.

$$\mathrm{Sc} = \frac{\mu_a}{\rho_a \delta} \tag{2.17}$$

$$\mathrm{Pr} = C_p \frac{\mu_a}{k_a} \tag{2.18}$$

where, μ_a and k_a are dynamic viscosity and thermal conductivity of air at temperature T_a, and have been determined from the property data given by US National Institute of Standards' REFPROP database (NIST, USA).

The mass diffusivity of water vapor in air δ, has been estimated from the relation developed by Bird et al. (1960).

$$\delta = 2.495 \times 10^{-5} \left(\frac{T_a}{292.88} \right)^{2.334} \tag{2.19}$$

Boundary conditions

The simulation model of humidification and initial condition for simulation are shown in Fig. 2.4 and Table 2.2. The cathode channel

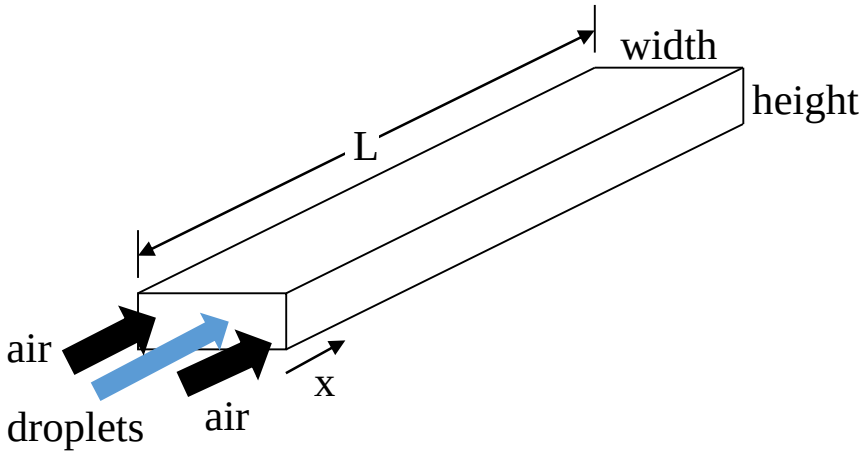

Figure 2.4 Simulation model of humidification

Table 2.2 Simulation condition of humidification

Parameters	Value	Notes
Cathode stoichiometry	2	
Current density	1.0 A/cm^2	
Cell active area	100 cm^2	
Initial water droplet velocity	3 m/s	
Relative humidity of inlet air	5%	dry condition
Channel length, width, height	500, 3, 3 (mm)	Duct shape
Inlet temperature of air	60°C	
Inlet temperature of droplets	50, 55, 60, 65 (°C)	
Channel wall temperature (cell)	65°C	

dimensions were 500 mm × 3 mm × 3 mm. The air velocity was calculated with mass flow rate supplied by air blower and area of cross section of chamber. In fuel cell's operating condition, ambient air is supplied to fuel cell. So the humidity of supplied air was fitted to ambient dry air condition.

2.2.3 PEM fuel cell model

A PEM fuel cell model is constructed based on following assumptions.

- A single cell with active area of 100 cm^2
- Uniform temperature of gas diffusion layer (GDL) and membran
- Nafion® 112 is used for membrane
- Electro-osmotic drag and back-diffusion are compensated each other

Open circuit voltage (OCV)

If the water product is in vapor phase, OCV is calculated as follows. Eq. (2.20) is a basic reaction for the hydrogen fuel cells.

$$H_2 + \frac{1}{2}O_2 \rightarrow H_2O \tag{2.20}$$

In a fuel cell, Gibbs free energy of formation is represented by Eq. (2.21).

$$\Delta\bar{g}_f = \left(\bar{g}_f\right)_{H_2O} - \left(\bar{g}_f\right)_{H_2} - \frac{1}{2}\left(\bar{g}_f\right)_{O_2} \tag{2.21}$$

Gibbs free energy can be expressed as in Eq. (2.22), and Eqs. (2.23) and (2.24)

for each reactant can be substituted in Eq. (2.22).

$$\Delta\bar{g}_f(T) = \Delta\bar{h}_f(T) - T\Delta\bar{s}(T) \tag{2.22}$$

$$\bar{h}_f(T) = \bar{h}_{298.15} + \int_{298.15}^{T} \bar{c}_p dT$$

(2.23)

$$\bar{s}(T) = \bar{s}_{298.15} + \int_{298.15}^{T} \frac{1}{T}\bar{c}_p dT \tag{2.24}$$

Eqs. (2.25), (2.26) and (2.27) are pressure-constant specific heats for each reactant with temperature in Kelvin, which can be substituted into Eqs. (2.22), (2.23) and (2.24).

$$\bar{c}_{P,\mathrm{H_2O}} = 143.05 - 58.040T^{0.25} + 8.2751T^{0.5} - 0.036989T \tag{2.25}$$

$$\bar{c}_{P,\mathrm{H_2}} = 56.505 - 22222.6T^{-0.75} + 116500T^{-1} - 560700T^{-1.5} \tag{2.26}$$

$$\bar{c}_{P,\mathrm{O_2}} = 37.432 + 2010.2\times10^{-5}T^{1.5} - 178570T^{-1.5} + 2368800T^{-2} \tag{2.27}$$

Summarizing above equations, the reversible OCV for a hydrogen fuel cell is given by Eq. (2.28)

$$OCV = \frac{-\Delta\bar{g}_f}{2F} \tag{2.28}$$

Theoretical values of OCV obtained from the calculation based on the above equations show that the OCV curve decreases evenly as the reacting temperature rises.

Voltage Losses

Voltage losses are classified into ohmic loss, activation loss and concentration loss. Following equations are used in calculation of voltage losses in this study. Related parameters are explained in Table 1. Ohmic losses in a MEA can be expressed like Eq. (2.29) which sums voltage losses in anode, cathode and proton exchange membrane.

$$\eta_R(T) = i\sum\frac{1}{\sigma} = i\left(\frac{l_a}{\sigma_a} + \frac{l_m}{\sigma_m} + \frac{l_c}{\sigma_c}\right) \tag{2.29}$$

Ion conductivity of Nafion® used as proton exchange membrane in this study is a function of water content and temperature as shown in Eq. (2.30)

$$\sigma_m = 100\exp\left[1268\left(\frac{1}{303} - \frac{1}{T}\right)\right](0.005139\lambda - 0.00326) \tag{2.30}$$

Where $\lambda = 0.043 + 17.18a - 39.85a^2 + 36.0a^3$ for $0 < a \le 1$

$\lambda = 14 + 14(a-1)$ for $1 \le a \le 3$

Activation loss and concentration loss are expressed as in the following equations.

$$\eta_A(T) = \frac{RT}{2\alpha F}\ln\left(\frac{i + i_n}{i_0}\right) \tag{2.31}$$

$$\eta_C(T) = \frac{RT}{2\alpha F}\ln\left(1 - \frac{i}{i_l}\right) \tag{2.32}$$

Polarization curves

Applying above OCV and voltage losses, operating voltage of a unit cell

can be expressed as in the following equation

$$V = OCV - \eta_R - \left(\eta_{A,anode} + \eta_{A,cathode}\right) - \left(\eta_{C,anode} + \eta_{C,cathode}\right) \quad (2.33)$$

Although OCV decrease as the cell temperature rises, total voltage losses are reduced enough to raise overall operating voltage as shown in Fig. 4.

For the same level of power, operation at high voltage results in low current density of the fuel cell, which leads to a low fuel consumption of the fuel cell. Low fuel consumption means a good efficiency of the fuel cell system. Table 2 shows a fuel consumption rate according to the operating temperature of the fuel cell. Even though the stack efficiency is good at high operating temperature, stack operation at high temperature is greatly restricted by durability and ion conductivity of membranes. As the ion conductivity of membranes depends on the water activity, high temperature operation is possible when adequate humidification methods are applied. Moreover, as the heat and water balance of the system are largely influenced by the operating temperature, the stack operating temperature is usually maintained at about 60℃ ~80℃ for Nafion® membranes. Recently, by the advent of some high temperature membranes like NFB (newly found fluorine- based) ion-exchange polymer composites or PBI class membranes, it is expected that stack operation at high temperature over 100℃ could be realized. When the fuel

cell is operated at high temperature over 100℃, heat releasing problems would be easily solved without large and complicated heat release devices. Moreover, humidification can be simplified.

2.3 Simulation results

2.3.1 Atomizer performance

Figure 2.6 shows calculation result of the air assist nozzle by eq. (2.3). Figure 2.6 (a) shows droplet size with change of air to liquid ratio (ALR) for various pressure differences and figure 2.6 (b) shows droplet size with change of nozzle diameter for various ALRs. As shown in this figure, very fine droplets are produced from the nozzle under all the considering conditions. And droplet size decreases with increase of pressure difference, ALR and lower nozzle diameter. Atomization performance is important factor for droplet evaporation and water evaporation directly affect the PEM fuel cell performance. Hence, it is important to maintain proper pressure difference and air to liquid ratio. In addition, the nozzle should be selected properly considering capable air and water flow rates.

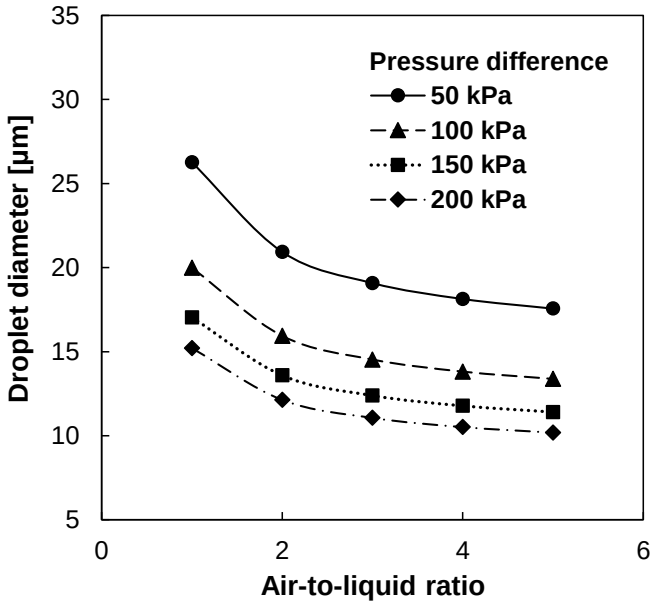

(a) With change of ALR for various pressure differences

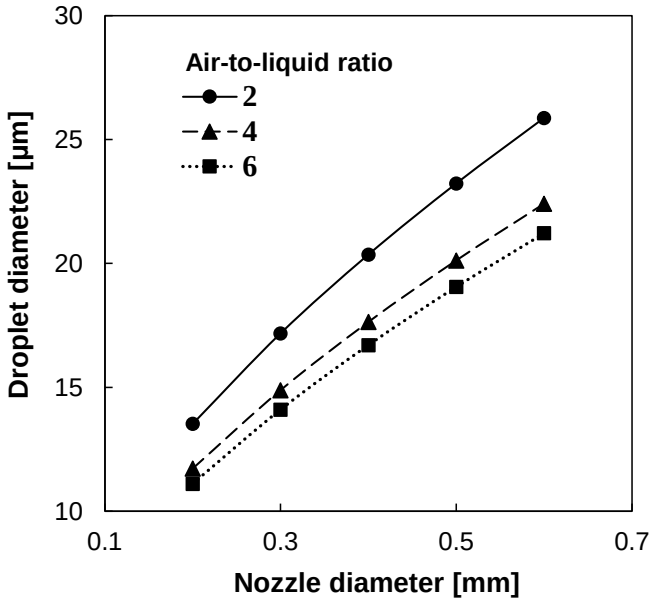

(b) With change of nozzle diameter for various ALRs

Figure 2.6 Calculation result of atomizer performance

2.3.2 Humidification performance

Numerical simulation of injector humidification was carried out according to the condition shown in Table 2.2.

Fig. 2.7 shows the result of simulation with air assist nozzle. The length of channel is 50 cm and active area is 100 cm^2 MEA (membrane electrolyte assembly). After passing through the cathode channel, droplet diameter with 50 μm attains dew point of 41.1°C, droplet diameter with 25 μm attains 48.0°C and droplet diameter with 10 μm attains 56.0°C. Because the lower droplet size is, the more evaporation of water occurs, hence, the dew point temperature of air increases. These results are not sufficient to operate PEM fuel cell systems. But it is comparable to the conventional humidifier, such as membrane humidifier, at high current range.

Effect of injected water temperature on the performance of humidification is shown in Fig. 2.8. Relative humidity of air which stands for the humidification performance increases as the water temperature goes up. Temperature of water is critical parameter for the performance, so it is important to minimize the heat loss and maintain the temperature of water which is supplied from water reservoir.

In Fig. 2.9, change of droplet size and mass fraction with increasing distance are showed at nozzle diameter of 0.4 mm. Droplet size decreases by

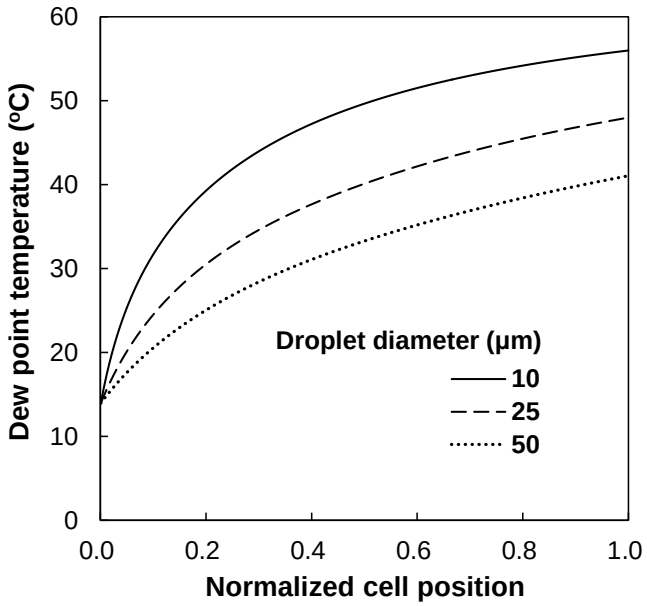

Figure 2.7 Change of dew point temperature of air with droplet size variation along the cathode channel

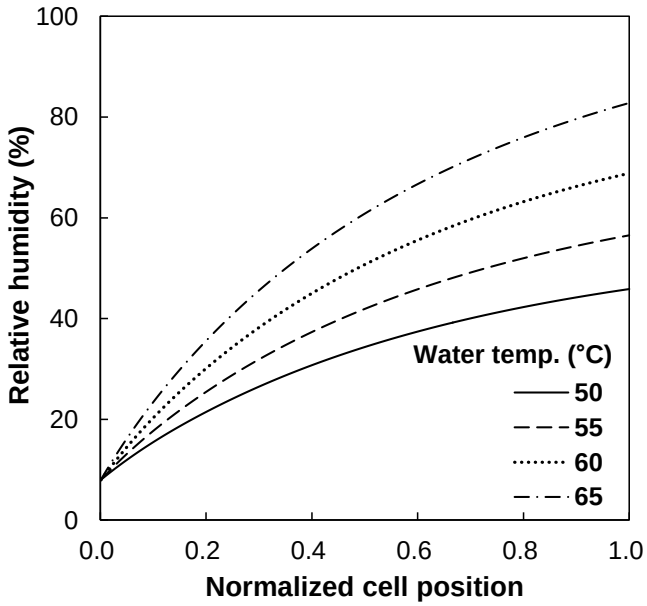

Figure 2.8 Change of relative humidity of air with water temperature along the cathode channel

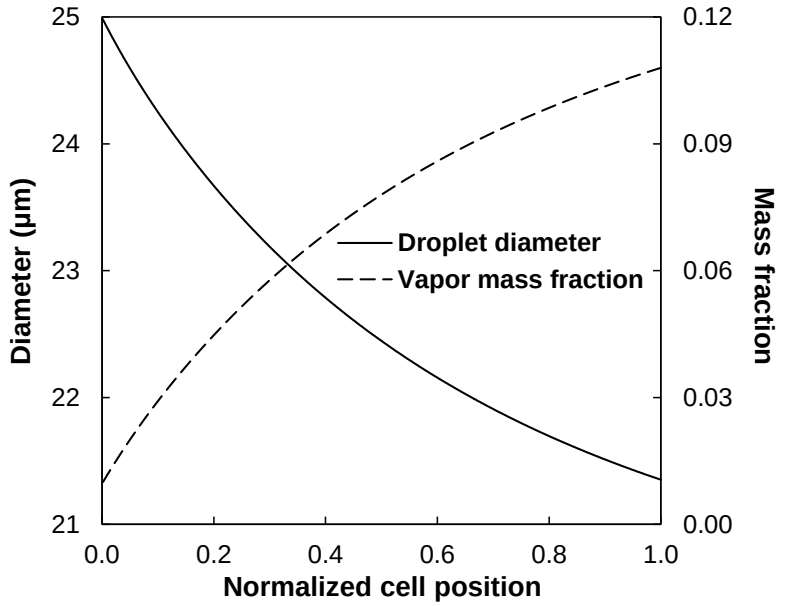

Figure 2.9 Change of vapor mass fraction and droplet diameter along the cathode channel

evaporation of water at the droplet surface and vapor mass fraction increased due to water evaporation After passing through the cathode channel, droplet size becomes about 21.5 μm. It can cause water flooding when the droplet collides into the channel wall or GDL surface. To prevent water flooding problem, it is necessary to control the water injection flow rate or timing.

2.4 Summary

In chapter two, numerical simulation of humidification performance using atomizer is mainly discussed. In order to carry out this simulation, an atomizer suitable for PEM fuel cell systems was investigated and water evaporation in the cathode channel was modeled numerically. Finally, from the result of the atomizer and the humidification model, PEM fuel cell performance was simulated.

Chapter 3. Fundamentals of direct water injection system and feasibility test

3.1 Introduction

In this chapter, a direct water injection system using an air-assist nozzle was developed. The development of direct water injection system is divided into two parts. The first is application of the atomizer to air-providing part of PEM fuel cell. And the second is to develop an evaluation method for humidification and evaporative cooling performance. Feasibility test of the direct water injection system was conducted with large area PEM fuel cell stack of 250 cm^2. Before stack experiments, water atomization performance of the selected air-assist nozzle was carried out by using a laser diffraction sensor. Then, the tests of the water injection system on the humidification and evaporative cooling performance were carried out at high current density region with dry air assuming in harsh operating conditions.

3.2 Development of direct water injection system

3.2.1 Application of the atomizer to air-providing part

Figure 3.1 shows a schematic diagram of the assembly of the air-assist atomizer and air-providing tubes with an external diameter of 25.4 mm (1 inch), which tubes are connected to the cathode inlet. In positioning the atomizer in the air-providing system, the first concern is ensuring that the central axis of the nozzle and the air-providing tubes coincide, as shown in Fig. 3.1. The reason for this is that when droplets impinge forcefully with the inner surfaces of the air-providing tubes, the droplets will combine at the surface, forming liquid water, so they cannot be introduced into the stack in the form of fine droplets. The assembly is a combination of air-providing tubes from the bubbler humidifier and the atomizer, with a compressed air flow line and separate liquid water flow line. The rate of air flow into the nozzle (the secondary air flow line in Fig. 3.1) is fixed to maintain the same pressure difference of 50 kPa. To provide the proper amount of air for the SR of the PEMFC stack, the remaining air flow is supplied through the primary air flow line. Consequently, the total air flow supplied to the cathode inlet is the sum of the primary and second air flows. The other important role of the

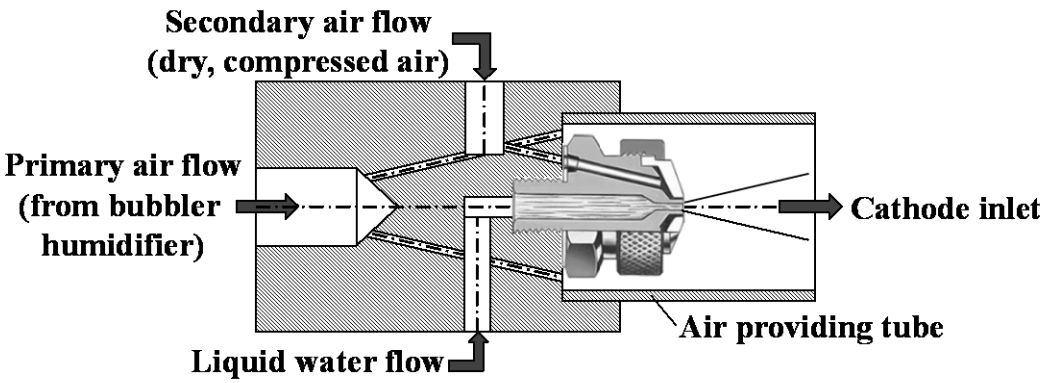

Figure 3.1 Assembly of atomizer and air-providing tube at the cathode inlet

primary air flow line is to control the humidification conditions. The air tank provides very dry air at a dew point temperature below -20℃. Providing this air without any humidification is inconsistent with the actual operating conditions of the PEMFC. So, the bubbler humidifier provides the air flow with water vapor to control the relative humidity (RH) of the cathode inlet, considering the low humidity of the ambient air. Finally, the liquid water is introduced into the nozzle in a precise manner by the liquid mass flow controller (MFC).

3.2.2 Performance evaluation method

To evaluate the performance of the direct water injection system using air assist nozzle, particularly the evaporative cooling performance, analyzing method is investigated. The key point of a quantification of evaporative cooling performance is to detect a dew point change at the cathode outlet. Figure 3.2 shows measured and theoretical values which can be obtained from the stack experiments. The underlined values are obtained from calculation with combination of theoretical equations and measured values. For example, heat generated from the PEM fuel cell stack is calculated by theoretical equation that measured voltage and current are used for this.

In this figure, to quantify evaporative cooling performance the best important thing is measuring dew point temperature of the cathode outlet. From the dew point temperature of the cathode outlet we can know partial vapor pressure then mass of water vapor per unit mass of dry air (g/kg) is calculated. Comparing dew point temperature of the cathode outlet with injection/non-injection condition, evaporation flow rate of injected water can be obtained. The enthalpy change of evaporated water time evaporation flow rate means evaporative cooling rate (i.e. heat rejection rate by evaporative cooling).

Another consideration is also required to investigate the evaporative cooling performance. This is a composition change of the cathode air. Generally, normal atmospheric air is supplied to cathode inlet and oxygen is consumed inside the fuel cell due to chemical reaction. Because oxygen is consumed along the cathode channel, air composition at the cathode outlet changes. When calculate a humidity ratio, mass of water vapor per unit mass of dry air, molecular weight ratio between gas and water vapor should be calculated first. Figure 3.3 shows change of air composition at the cathode inlet/outlet when stoichiometry ratio is 2

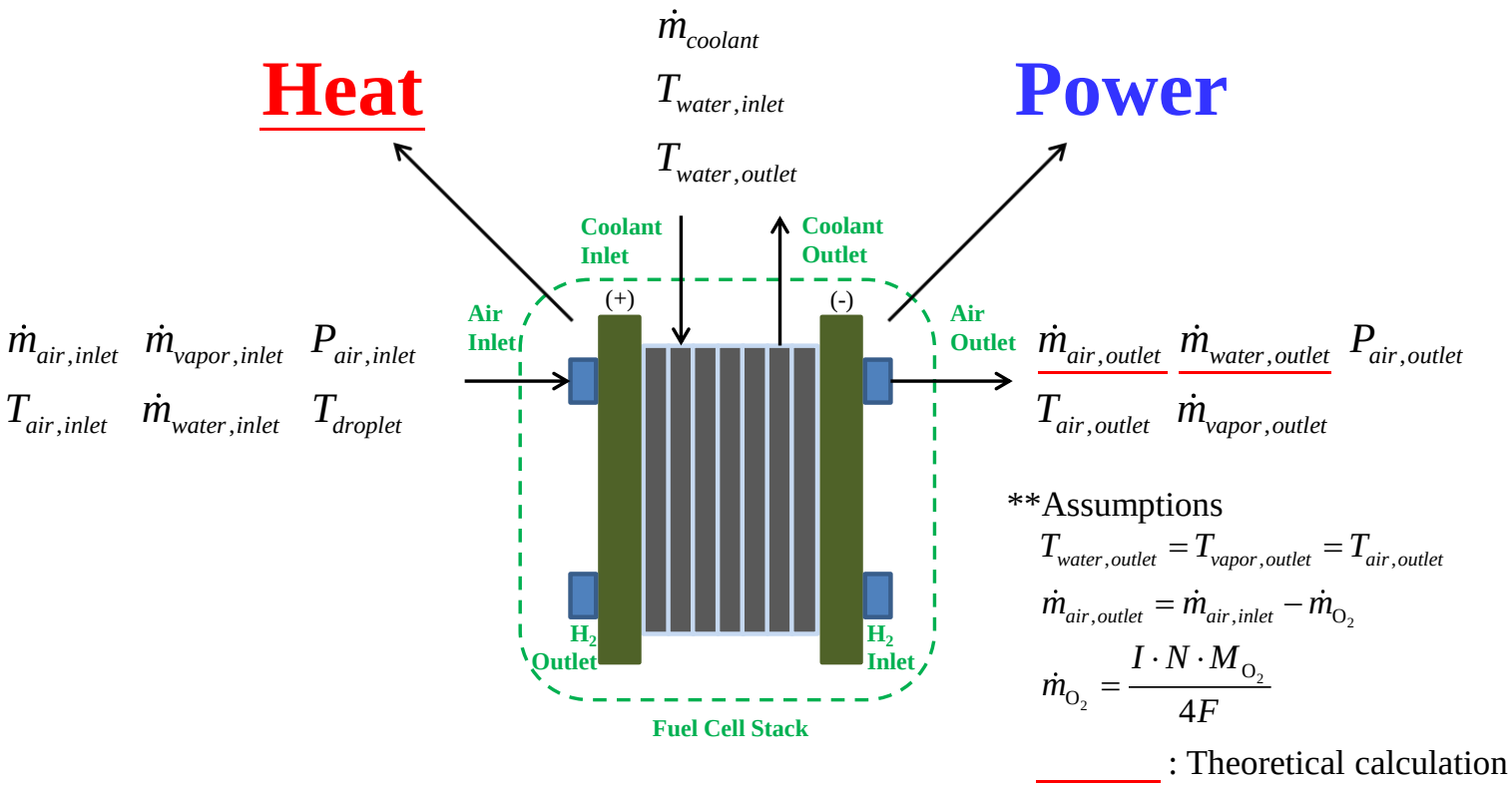

Figure 3.2 Measured and theoretical values of the stack experiments

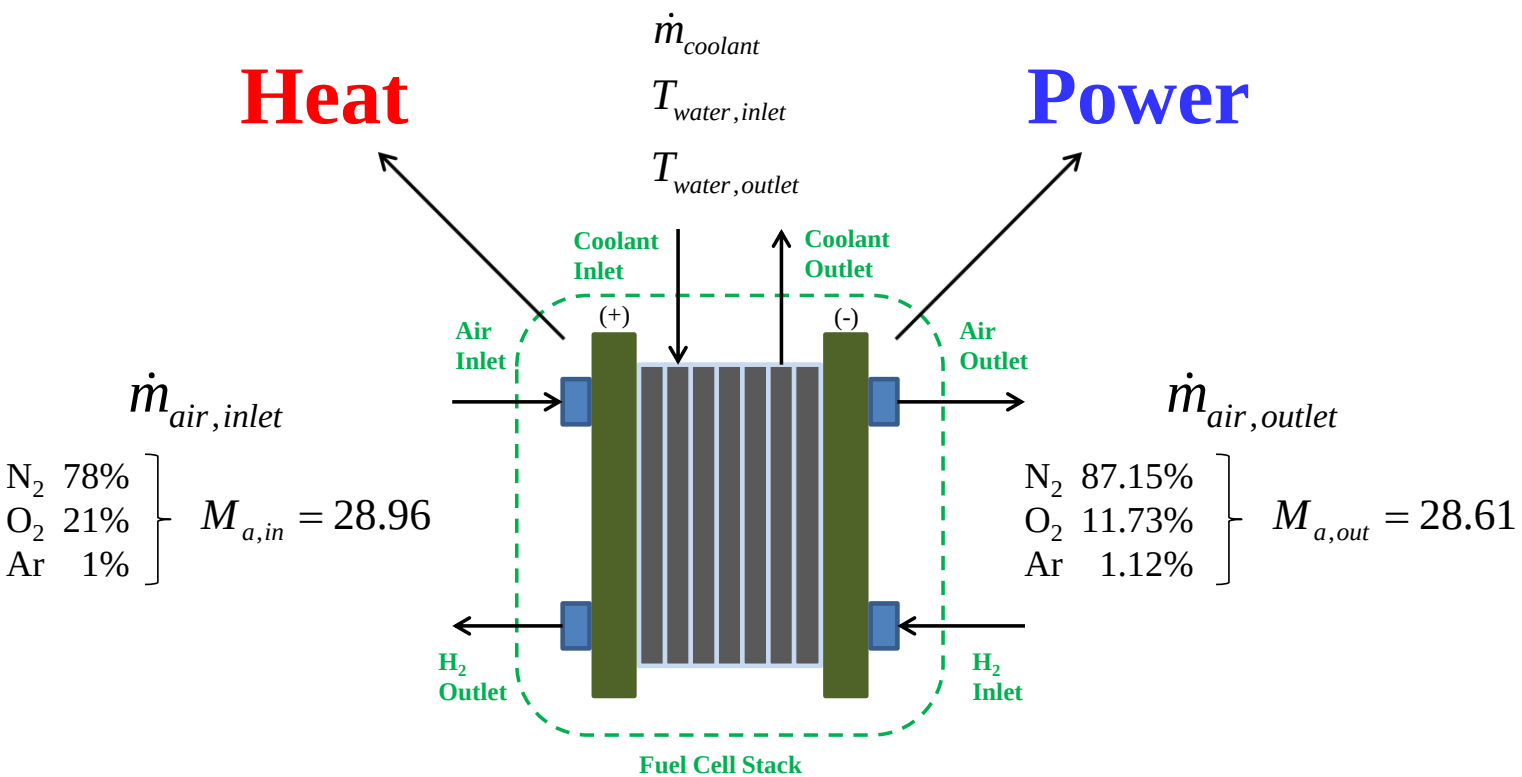

Figure 3.3 Change of air composition at the cathode inlet/outlet when stoichiometry ratio is 2

3.3 Feasibility test

3.3.1 Water atomization performance

Before experiments were conducted using the stack described in the previous section, the atomization performance and characteristics of the air-assist nozzle used in this study were investigated. Figure 3.4 shows the measurement device and the principle of droplet size distribution. In this study, the measurement results obtained using a laser diffraction method (Sympatec, Clausthal-Zellerfeld, Germany, HELOS). Laser diffraction method is analyzing particle size distributions by measuring the angular variation in intensity of light scattered as a laser beam passes through a dispersed particulate sample.

Figure 3.5 show two case of droplet size distribution. Fig. 3.5(a) is a general result of the measurements that have uniform distribution. From eq. (2.3) and, the droplet size and the uniformity decrease when the pressure difference and the air to liquid ratio (ALR) are low. In this case, despite of low pressure difference of 50 kPa, droplets from the nozzle have uniform distribution. However, in Fig. 3.5(b), the droplet size distribution have another peak in large size region compared to Fig. 3.5(a). It means that the droplets

(a) Picture of measuring device: HELOS H2854

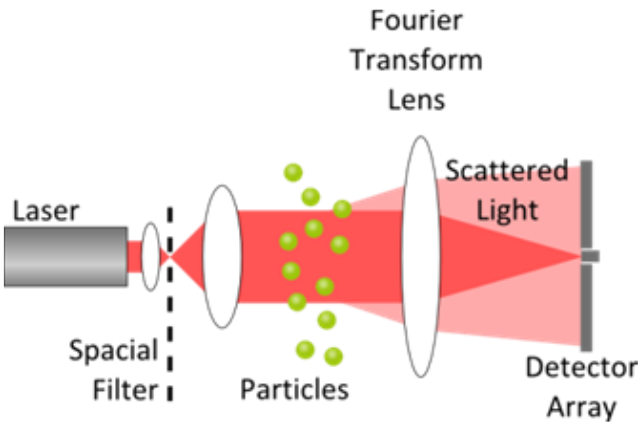

(a) Schematic diagram of laser diffraction method

Figure 3.4 Measuring device and the principle of droplet size distribution

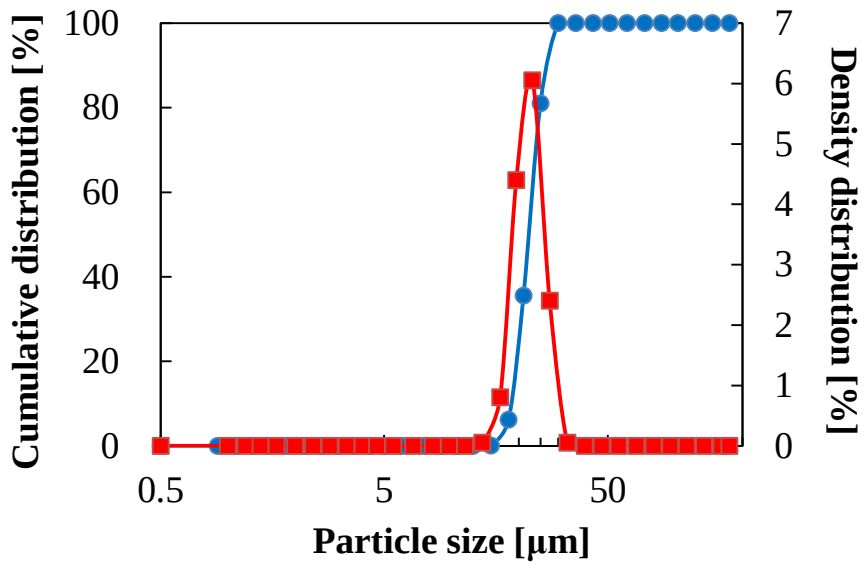

(a) pressure difference: 50 kPa, ALR: 1.68

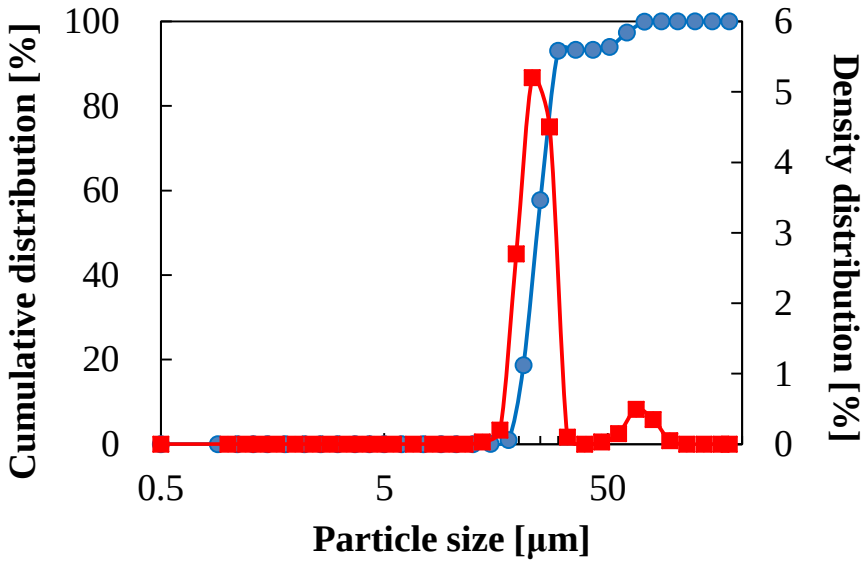

(b) pressure difference: 200 kPa, ALR: 0.49

Figure 3.5 Measured result of droplet size distribution

from the nozzle was less uniform than Fig. 3.5(a). This condition has high pressure difference of 200 kPa but also has very low ALR value of 0.49. From the result of Fig. 3.5, when the ALR value is too low, the uniformity of the spray dropped in spite of high pressure difference. In the Fig. 3.6, the measured value of Fig. 3.5(b) is not included because of its low uniformity.

Figure 3.6 shows the change in the droplet size in SMD with change in ALR for various pressure differences. Figure 3.6(a) shows the result of a calculation based on Eq. (2.3) and (b) shows measurement results. All of the property values used in the calculations were taken from the US National Institute of Standards' REFPROP database (NIST, USA).

In the measurements, the ALR ranges were confined to values less than 3 because of the limitations of the measurement device. Thus, the given conditions for the two cases were not exactly the same. Nonetheless, the measured data is useful for comparison with the values obtained from the calculation results. The calculated and measured values are somewhat different, the former being smaller in most cases. However, the two sets of data exhibit the same trends with respect to the effects of the ALR and the pressure difference on the droplet size; the larger the ALR and the pressure difference are, the smaller the droplets produced by the nozzle. Moreover, the results show that very fine droplets, less than 25 μm in diameter, were

produced under all of the injection conditions considered.

In the measurement results, the effect of pressure difference on the droplet size when it is over 0.5 kPa is not that large compared to calculation results. And where the ALR is over 2, the droplet size varies only a little in calculation. Although there are not enough cases, speaking in terms of the effect of ALR, it is supposed that the tendency in measurement may be similar to the results of calculation. In the stack experiments, the pressure difference and the ALR were set to 50 kPa and over 2.5, respectively. For these conditions, the variation of droplet size must be very small, so the effect of droplet size on the humidification and evaporative cooling is not considered in this study.

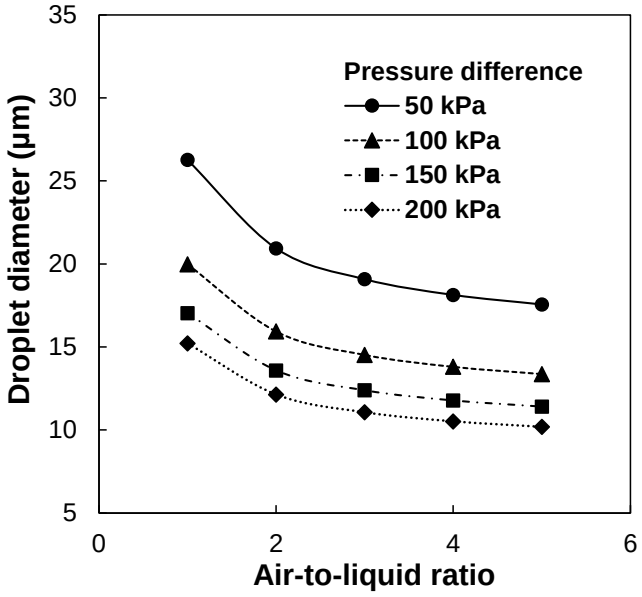

(a) calculation

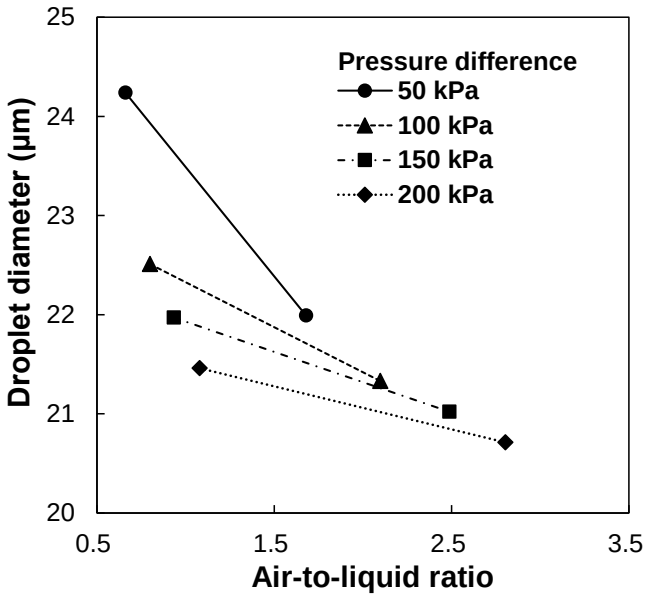

(b) measurement

Figure 3.6 Droplet diameter with change in the air-to-liquid ratio for various pressure differences when the nozzle orifice diameter is 0.4194 mm

3.3.2 Experimental

Experimental setup and measurement

Figure 3.7 shows a schematic diagram of the experimental setup. The experiments were conducted with a five-cell fuel cell stack with an active area of 250 cm^2. Using air and hydrogen MFCs, the cathode/anode SR numbers are adjusted. The relative humidities of the cathode/anode inlets are controlled through the bubbler humidifier. The temperatures at the cathode/anode inlets are controlled by the line heater that wraps around the tube lines. Although water can be supplied to the nozzle by siphoning without any water-providing device, the liquid MFC is used to control both the water flow rate and the atomization performance of the nozzle. The electronic load (Kikusui Electronics Corp., Yokohama, Japan, PLZ1004W and PLZ2004WB, accuracy in constant-current mode: ±1.2% of setting, ±1.1% of full scale) draws current and consumes electrical energy from the fuel cell stack in constant-current mode. Experimental data, including single-cell voltages, were collected using a data acquisition unit (National Instruments, Austin, Texas, USA, cDAQ-9172 and various modules). The dew point temperature was measured using chilled-mirror-type hygrometers (Azbil corp., Tokyo, Japan, FDP-SP). During operation of the system, there is a relatively large amount of liquid water in the stream at the cathode outlet because of water injection. Therefore, to

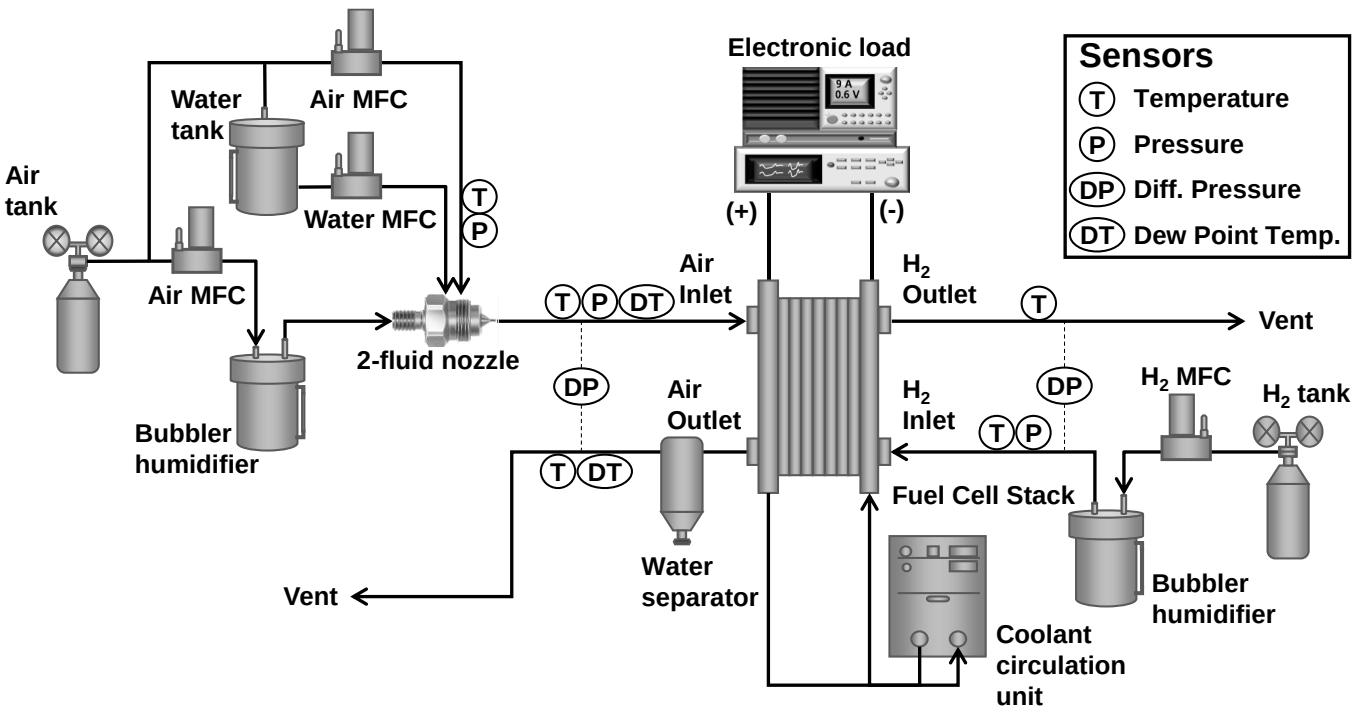

Figure 3.7 Schematic diagram of the experimental setup

Table 3.1 Measurement accuracy of sensors

Sensors	Model	Manufacturer	Measurement accuracy
Thermocouple	T-type	-	± 0.3℃
Resistance temperature detector	Pt 100 Ω	-	± 0.1℃
Dew point hygrometer	FDB-SP	Azbil	± 0.5℃
Mass flow controller (air)	F-202AV, F-201C	Bronkhorst High-Tech	± 0.5% of reading ± 0.1% of full scale
Mass flow controller (H2)	F-201C	Bronkhorst High-Tech	± 0.5% of reading ± 0.1% of full scale
Mass flow controller (water)	M13 V14I	Bronkhorst High-Tech	± 0.2% of reading ± 0.2 g/h zero stability
Mass flow meter (coolant)	ULTRAmass MKII	Oval	± 0.2% of reading
Pressure transmitter (nozzle)	S-10	WIKA	± 0.25% of full scale
Pressure transmitter (others)	PSH	Sensys	± 0.15% of full scale
Differential pressure transmitter	3051CD	Rosemount	± 44 Pa
Voltage sensor (single cell voltage)	NI9215	National Instruments	± 0.02% of reading

remove fluctuations and enhance the accuracy of the measurement of the dew point temperature, a water separator (SMC corp., Noblesville, Indiana, USA, AMG150C) was installed just before the dew point hygrometer. This cyclone water separator removes 99% of the liquid water in the incoming flow except the vapor phase. Deionized water coolant is supplied from a thermostatic bath by a pump. The accuracy of the sensors, their manufacturers, and model names are given in Table 3.1.

Experimental conditions

The experimental conditions are summarized in Table 3.2. To investigate the effects of temperature on the evaporation of injected water, two stack operating temperatures were considered: 60 and 70℃. The operating temperature of the stack is controlled by coolant circulation, and the coolant flow rate was fixed at 5 l/min. This is the maximum flow rate of the circulation pump that enables minimization of the temperature difference between the coolant inlet and outlet. Hydrogen (H2) is supplied at the operating temperature of the stack and 100% RH, with an SR of 1.5. Air is supplied at the same temperature with an SR of 2.0, and its RH is fixed at 20%, considering the low humidity of the ambient air without additional humidification.

Table 3.2 Operating conditions in the experiments

Operating parameters	Values
Operating temperature (℃)	65
Operating pressure (bar)	1
Coolant flow rate (l/min)	5
Relative humidity (%)	Cathode (air): 20
	Anode (H2): 100
Reaction gas stoichiometric ratio	Cathode (air): 2.0
	Anode (H2): 1.5
Pressure difference of the nozzle (kPa)	50
Water injection flow rate (mL/min)	1, 3, 5
Temperature of injected water (℃)	40
Operating current density (A/cm^2)	0.8, 1.0, 1.2

The nozzle orifice diameter is 0.4194 mm. The pressure difference between the air inlet and the injection orifice was fixed at 50 kPa. Although the atomization performance of the nozzle is better when the pressure difference is higher, larger pressure differences require more power consumption. The water injection flow rates from the nozzle were set to 1, 3, and 5 ml/min, based on the maximum water production rate of the stack, because the system was designed assuming that the water required for injection would be provided from the water produced in the PEMFC stack, as mentioned previously. The theoretical maximum water production rate, including both the liquid and vapor phases, was taken to be 0.140 g/s (= 8.40 ml/min at 20℃) at a current density of 1.2 A/cm^2. Considering the occurrence of condensation with decreasing temperature at the cathode outlet and its storage during non-injection situations at low current densities, a maximum usable water flow rate of 5 ml/min was thought to be reasonable. The temperature of the injected water was set to 40℃, assuming that the water in the storage tank at the cathode outlet would be at this temperature. All of the experiments were conducted at high current densities (0.8, 1.0, or 1.2 A/cm^2) within the range corresponding to high heat rejection and humidification loads.

Experimental procedure

In the stack performance test using direct water injection method, it should be noted that the water at the cathode flow channel should be removed before every experiment to insure that the effects of water injection are measured accurately. This water removal was progressed until the humidity at the cathode outlet reached a steady state using a large amount of low-humidity air with zero current (i.e. without electrical load). And the current was then increased to be within the target high current density region. When the current reached the desired value, it was maintained until the stack performance reached a steady state. Water injection was then begun. While liquid water was being injected into the cathode inlet of the stack, changes in the stack performance and the dew point temperature of the cathode outlet were monitored.

3.3.3 The effects of direct water injection method

Fundamental considerations

Figure 3.8 shows changes in the average cell voltage and dew point temperature of the cathode outlet for an operating temperature of 65℃, a current density of 1.0 A/cm^2, and a water injection flow rate of 5 ml/min. As

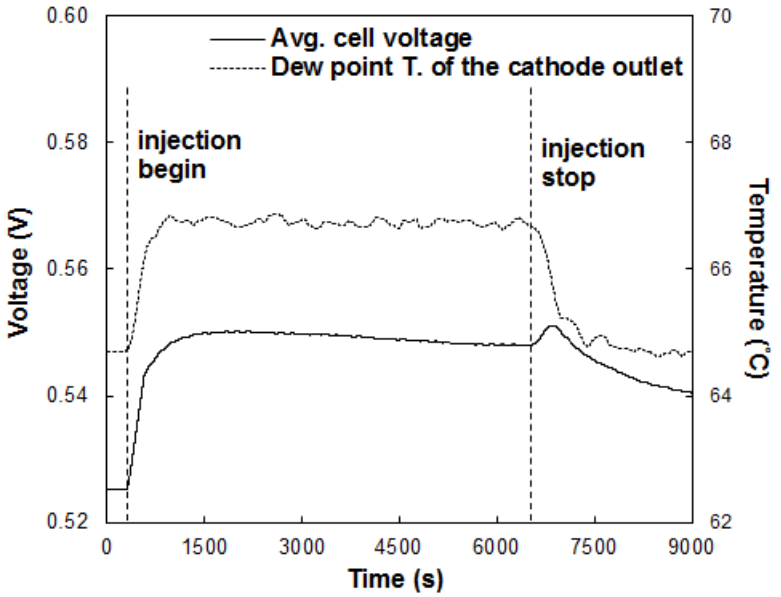

Figure 3.8 Changes in average cell voltage and dew point temperature at the cathode outlet at an operating temperature of 65℃, current density of 1.0 A/cm^2 and water injection flow rate of 5 ml/min

Fig. 3.8 shows, the fuel cell stack is in a steady state before the water injection begins. Immediately after the water injection begins, the stack voltage and the dew point temperature of the cathode outlet increase, indicating that the injected water evaporates through the cathode flow channel. The rise in the dew point temperature of the cathode outlet is a clear proof of the evaporation of the injected water. The increase in the average cell voltage reflects the humidification effect of water injection, but it cannot be concluded that this effect is due only to the water vapor. It is in fact the result of membrane hydration by both the water vapor and the liquid water. On the other hand, because the dew point temperature is a parameter that represents the amount of water vapor in the gas stream, the increase in the dew point temperature of the cathode outlet can be attributed to the evaporation of the injected water only. Therefore, the evaporation rate of the injected water can be determined from the difference in the humidity ratio at the cathode outlet before and after the water injection begins, as shown in the following equation.

$$\dot{m}_{evap} = \dot{m}_{air,\,out} \cdot \Delta w \tag{3.1}$$

In Eq. (3.1), $\dot{m}_{air,\,out}$ is the mass flow rate that exiting air at the cathode outlet and it can be expressed in following equation.

$$\dot{m}_{air,\,out} = \dot{m}_{air,\,in} - \dot{m}_{O_2} \tag{3.2}$$

In Eq. (3.1), Δw is a change of the humidity ratio at the cathode outlet and the humidity ratio at the cathode outlet is defined as the mass of water vapor per unit mass of dry air (g_w/kg_{da}). It can be calculated from the following equations.

$$w = \frac{m_w}{m_a} = \frac{M_w P_w}{M_a P_a} = A\frac{P_w}{P_a} = \frac{A \cdot P_w}{(P - P_w)} \tag{3.3}$$

$$A = \frac{M(\mathrm{H_2O})}{M(\mathrm{air})} \cdot 1000 \tag{3.4}$$

In Eq. (3.3), P_v is equal to the P_{ws} corresponding to the dew point temperature at the cathode outlet, which can be calculated from the "Wagner, Pruß" formula. In applying the value of $M(\mathrm{air})$ to Eq. (3.4), it should be noted that the molecular weight of the exhaust gas at the cathode outlet is different from atmospheric air. Because of oxygen consumption in the fuel cell stack, the exhaust air composition changes. For an SR of 2.0, considering oxygen consumption on the cathode side, and $M(\mathrm{exhaust\ air})$ of 28.60 g/mol, the molecular weight ratio in Eq. (3.4) becomes 0.630.

Figure 3.9 shows changes in the coolant temperature of the stack inlet/outlet and the heat rejection rate by the coolant. Deionized water is used as a coolant in this study and the heat rejection rate can be calculated from Eq. (3.5).

$$Q_{\mathrm{coolant}} = \dot{m}_{\mathrm{coolant}} \cdot C_{\mathrm{p,\ coolant}} \cdot \Delta T_{\mathrm{coolant}} \tag{3.5}$$

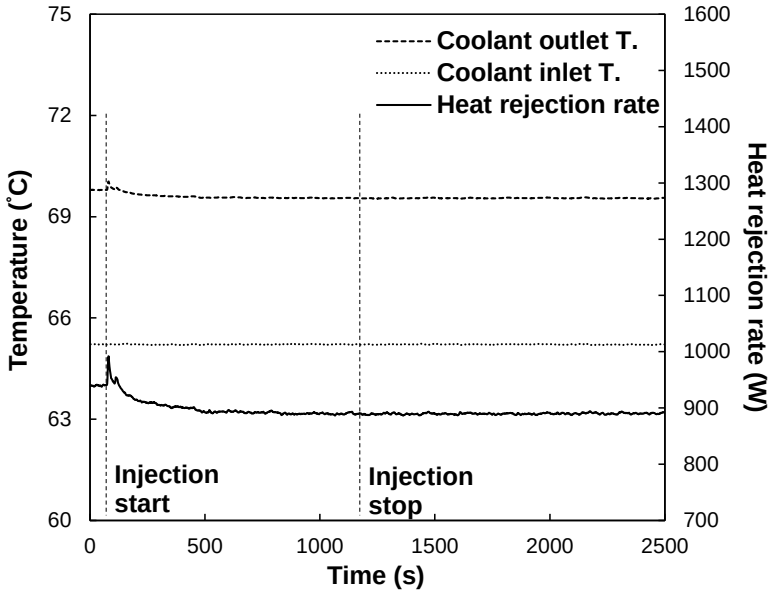

Figure 3.9 Changes in coolant temperature at the stack inlet/outlet and heat rejection rate by coolant at an operating temperature of 65℃, current density of 1.0 A/cm^2 and water injection flow rate of 5 ml/min

In this experiment, before water injection begins, the stack efficiency is very low because of insufficient cathode humidification by the supplied air, which has an RH of 20%. Accordingly, as Eq. (3.6) shows, there is considerable heat generation by the fuel cell.

$$Q_{\text{stack}} = (1.253 - V_{\text{cell}}) \cdot N \cdot I \tag{3.6}$$

In Eq. (3.6), 1.253 is the voltage equivalent of the lower heating value (HHV), also called the thermal cell voltage. In this situation, when water injection begins, the heat generation rate decreases because of the efficiency enhancement caused by the humidification effect. In addition, because of the evaporative cooling achieved by the water injection, the stack temperature decreases. This is reflected in the decrease in the coolant outlet temperature, which also implies that the heat rejection load of the coolant radiator decreases.

Humidification effect

The humidification level affects the fuel cell performance directly, so the humidification effect can be assessed by comparing the average cell voltages with and without water injection. Figure 3.10 shows the fuel cell performance at operating temperatures of 60 and 70℃ for various water injection flow rates and high current densities. The lower 4 lines of this figure are average

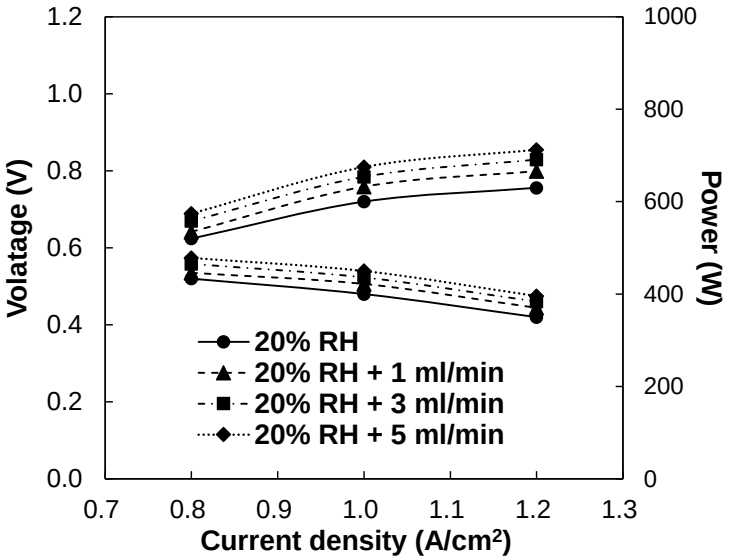

(a)

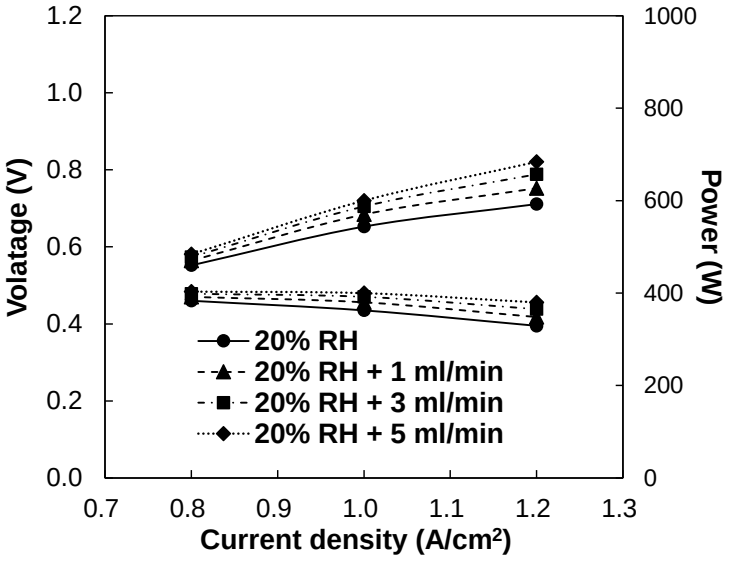

(b)

Figure 3.10 Stack performance for a given operating temperature for various water injection flow rates at high current densities; (a) 60℃, (b) 70℃.

cell voltage curves and the upper 4 lines are electric power curves. The electric stack power is as following equation.

$$P_{el} = V_{cell} \cdot N \cdot I \tag{3.7}$$

The effects of residual water

Referring again to Fig. 3.8, after the water injection is stopped, the stack output voltage gradually decreases and reaches a value that is higher than that before the water injection began. This indicates that after the water injection stops, residual liquid water at the cathode flow channel is used for humidification. The dew point temperature of the cathode outlet drops sharply after the water injection stops and reaches a value lower than that of the initial state. This is due to stop of water injection and also attributed to the effect of the residual liquid water. In general, at the cathode flow channel, the air near the outlet side is almost saturated due to evaporation of water produced by the reaction between H_2 and O_2. In this situation, liquid water located in various places at the cathode channel facilitates condensation of the surrounding vapor due to the cohesive nature of water. For this reason, after injection stops, the amount of water vapor in the cathode exhaust gas decreases temporarily. After a while, however, the dew point temperature increases over time because of evaporation of the residual water by the cathode air flow. When all

of the residual water evaporates, the dew point temperature will return to its initial value of before injection.

Figure 3.11 shows changes in the average cell voltage and the dew point temperature of the cathode outlet at an operating temperature of 60℃, a current density of 1.2 A/cm^2, and a water injection flow rate of 5 ml/min. This is an example of a case in which water removal from the stack was not performed before the water injection. As Fig. 3.11 shows, the average cell voltage and the dew point temperature of the cathode outlet rise in a manner similar to that shown in Fig. 3.8. However, in this case, the improvement in the stack performance is very small. Because the initial value of the average cell voltage shown in Fig. 3.10 (approximately 0.496 V) is considerably higher than the value for non-injection conditions and a main air stream with an RH of 20% (approximately 0.478 V, as shown in Fig. 3.10). This is attributed to the humidification effect of residual water that was not removed from the fuel cell stack. Furthermore, the maximum cell voltage (approximately 0.523 V) is lower than after water removal (approximately 0.540 V, as shown in Fig. 3.10). And the increased voltage continues to decrease that does not maintain a steady state. This situation is similar to a flooding phenomenon which is a typical problem of PEM fuel cells]. It is believed that because the number of reaction sites decreases due to a local

blockage by liquid water at the cathode channel or gas diffusion layer (GDL). The sudden rise in the dew point temperature at 450 s can also be interpreted as an influence of the flooding. It is result of an instantaneous discharge of water vapor which kept inside the cathode channel due to a local blockage by flooding.

Finally, as Fig. 3.10 show, the stack performance increase with increased current density. Because an increase in the current density corresponds to an increase in the air flow rate for a fixed SR, evaporation of the injected water is facilitated by increasing the heat and mass transfer rates. Although the water production rate increases with increasing current density, which has a negative effect on the evaporation of injected water, it is thought that the effect of an air flow rate increase is greater.

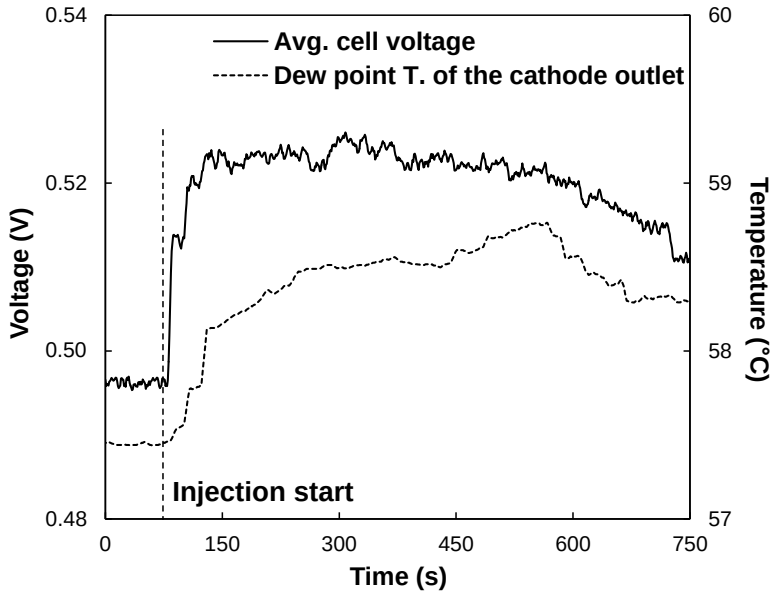

Figure 3.11 Changes in average cell voltage and dew point temperature at the cathode outlet without water removal process at an operating temperature of 60℃, current density of 1.0 A/cm^2 and water injection flow rate of 5 ml/min

3.4 Summary

In this chapter, to eliminate the need for a bulky humidifier and to lighten the cooling load of PEM fuel cells, a simultaneous cathode humidification and evaporative cooling system using an external-mixing air-assist atomizer was developed, and its performance was investigated experimentally.

Measurement of the atomization performance indicated that the air-assist nozzle produced very fine droplets, 20 to 25 μm in diameter, at a pressure difference of 50 kPa and the given air-to-liquid ratios. And due to its small variation of droplet diameter, the effect of droplet size on the humidification and evaporative cooling is not considered in this study.

The results of the stack performance experiments show that the direct water injection method proposed in this paper is quite effective in cathode humidification. This system takes only a small volume and able to humidify in an active manner unlike to other passive humidifiers such as membrane humidifier. The stack performance improved with an increased water flow rate because of the increased humidification effect. At a given water flow rate, the improvement in the stack performance that can be attributed to the humidification effect was greater when the operating temperature was lower.

Chapter 4. Operating characteristics of PEMFCs with a direct water injection system

4.1 Introduction

In this chapter, the operating characteristics considering various relating variables were investigated to provide useful information and better understanding on PEM fuel cells with direct water injection system. Water injection flow rate, water injection temperature, stack operating temperature, stack operating pressure and cathode stoichiometric ratio are considered in this chapter as operating variables. Methodology which uses measurement of current, voltage and dew point temperature is the same as the previous chapter. In addition, the experiments were performed at broader current range including low current regions.

4.2 Humidification performance

4.2.1 Experimental apparatus and test procedure

Figure 4.1 shows the schematic diagram of the experimental setup.

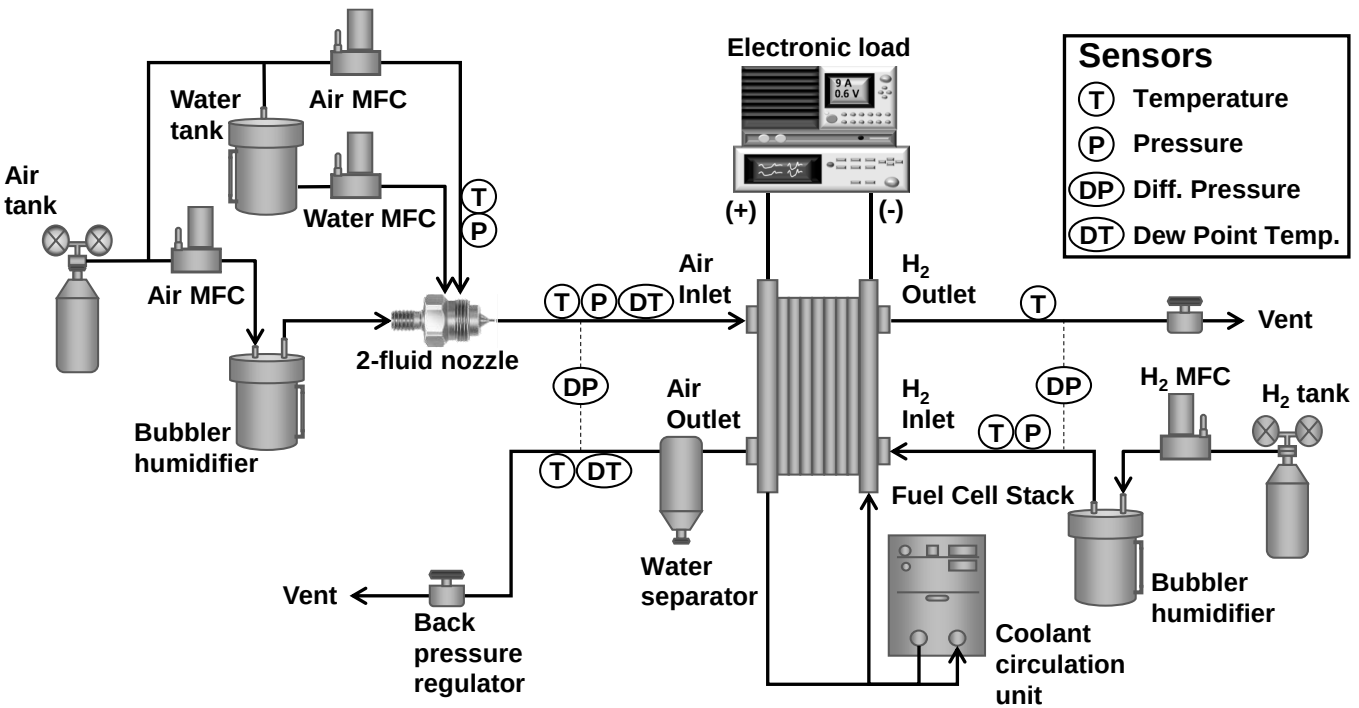

Figure 4.1 Schematic diagram of the experimental setup

Table 4.1 Operating conditions in the experiments

Operating parameters		Values
Operating temperature (℃)		60, 70
Operating pressure (bar)		1.0, 1.5, 1.8
Coolant flow rate (l/min)		3
Relative humidity (%)		Cathode (air): 20
		Anode (H2): 100
Reaction gas stoichiometric ratio		Cathode (air): 1.5, 2.0, 3.0
		Anode (H2): 1.5
Pressure difference of the nozzle (kPa)		50
Water injection flow rate (mL/min)		1, 3, 5
Temperature of injected water (℃)		25, 40, 60
Purge process	Gas flow rate (l/min) (cathode/anode)	50/2

Which is the same as the Figure 3.7 except for back pressure regulator at the cathode/anode outlet. These two devices were installed at the last of the outlet tubes to control stack operating pressures.

The experimental conditions are summarized in Table 4.1. In this chapter, water injection flow rate, water injection temperature, stack operating temperature, stack operating pressure and cathode stoichiometric ratio are considered as operating variables. Contrary to previous chapter, all the current ranges are concerned including low current region in this chapter. There are merit and demerit for water evaporation in both low and high current region. In low current region humidity inside the fuel cell is low, which is an advantage for water evaporation. On the other hand, in low current condition, amount of supplying air is small and temperature inside the fuel cell is low which are disadvantage for water evaporation. In high current region, the effects of humidity, temperature and air flow rate are the opposite in the low current region.

The experiment consisted of three processes. The first step is purge. The purge process was carried out over 2 hours with dry air which is corresponding to 20% relative humidity at operating temeperature. Then activation process to set the balanced GDL condition was conducted more than 3 cycles with dry air of 20% RH (100% RH H_2 for anode) until get the

uniform performance curve. Finally, the humidification performance with water injection was measured. In both activation and performance measurement processes, current density was changed every 0.1 A/cm^2. As shown in Fig. 4.2, in activation process the every current was maintained 2 minutes and in performance measurement process current duration time was changed depending on the situations. The situations mean water content in GDL and membrane. Figure 4.3 shows performance change with different water content in GDL and membrane. Normal purge means purge process with general atmospheric dry air of 20% RH. Dry purge is performed to dehydrate the GDL and membrane with totally dry air which dew point temperature is under -10°C. After dry purge the stack performance is very low because the membrane is nearly dehydrated condition. This condition is similar to non-activated new stack. Hence, it takes very long activation time more than 12 hours to obtain the maximum performance. The stack performance after normal purge is low than the maximum performance but the difference is not significant comparing to dry purge condition. And its activation time to maximum performance is also short. This figure means stack performance is different with water content or distribution in GDL and membrane, although the reactant gases have the same relative humidity. This phenomenon has greater effect on fuel cells with a large active area. Because

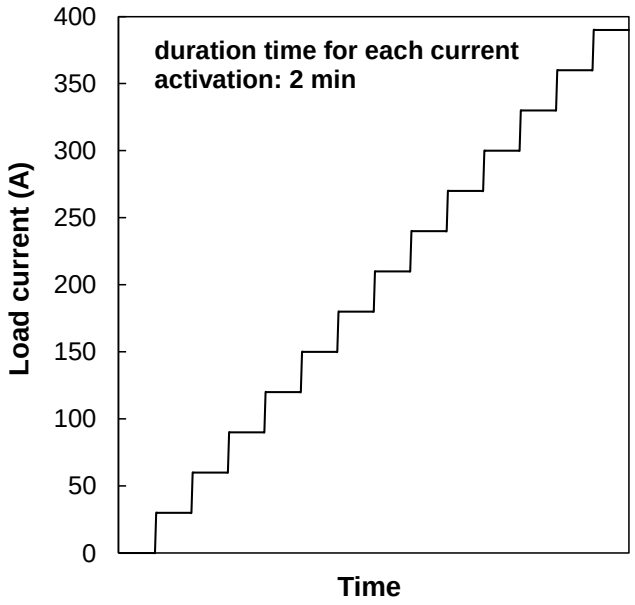

Figure 4.2 Load current cycle for activation and performance measurement process in balanced GDL and membrane condition

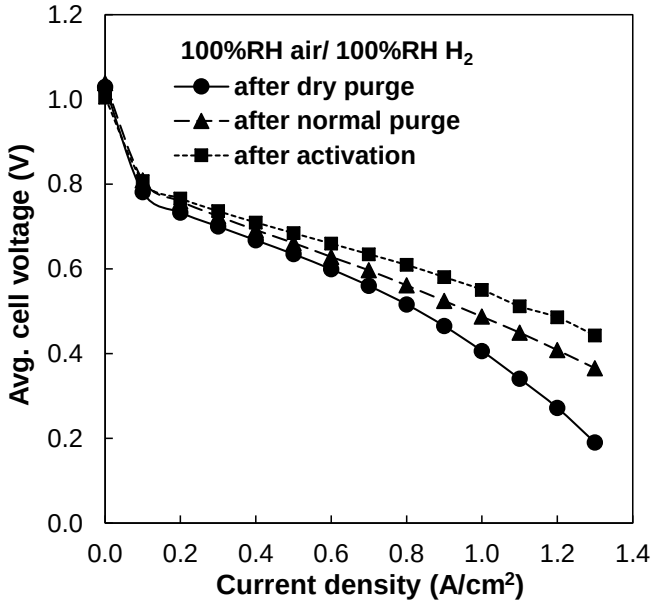

Figure 4.3 Stack performance with different water content and distribution inside the cathode

the fuel cells with large active area have long and complex channel and water distribution of low uniformity. For this reason, during performance measurement with water injection, purge process is performed to balance water content inside the cathode. And through a lot of load current cycles the performance was measured.

4.2.2 Water injection flow rate

Figure 4.4 shows performance curve with different water injection flow rates when the operating temperature is 60°C, operating pressure of 1 bar and injection water temperature is 40°C. As shown in this figure the stack performance increases with the rise of water injection flow rate. It is due to the more humidification effect with the higher water injection flow rate. In case of 5 ml/min injection, the stack performance at current density under 0.8 A/cm^2 is higher than that of 50% RH condition. However, when the current density is over 0.9 A/cm^2 the stack performance is lower than 50% RH case. The reason for this result is insufficient humidification. Figure 4.5 shows required water vapor to obtain the various target relative humidity of the cathode inlet air with SR 2. As shown in figure 4.5, at high current region more water vapor is required to get the same relative humidity. From this

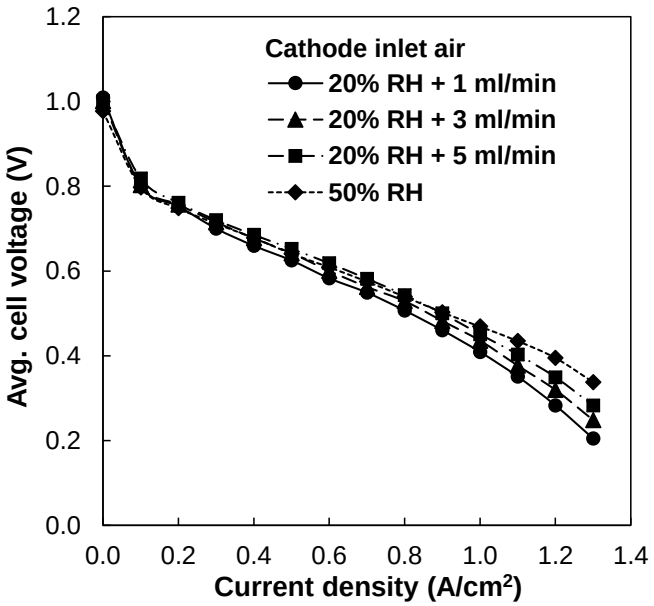

Figure 4.4 Stack performance with different cathode inlet air condition when the operating temperature is 60°C, operating pressure is 1 bar and injection water temperature is 40°C

result, we can know that it is necessary to apply different water injection flow rate with different current density. Comparing to 50% RH air, other cases also had lower performance and this effect was appeared at high current region. The slope change of the performance curve is reflecting this result.

4.2.3 Injection water temperature

Figure 4.5 shows performance curve with different injection water temperatures when the operating temperature of 60℃, operating pressure of 1 bar and water injection flow rate of 5 ml/min. Overall, there is no significant difference in the stack performance with change of injection water temperature. Comparing to the cathode air of 50% RH, the performance under 0.8 A/cm^2 is higher and that over 0.9 A/cm^2 is lower. However, there is a small performance change in high current density region. As shown in simulation result of the chapter 2, this is due to more evaporation with higher temperature of injection water.

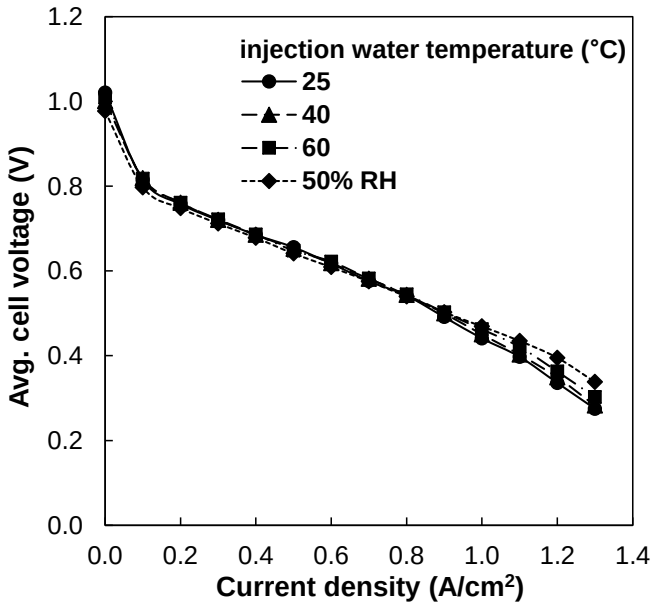

Figure 4.5 Stack performance with different injection water temperatures when the operating temperature is 60°C, operating pressure is 1 bar and water injection flow rate is 5 ml/min

4.2.4 Stack operating temperature

Figure 4.6 shows performance curve with different operating temperature when the operating pressure of 1 bar, water injection flow rate of 5 ml/min and injection water temperature of 40℃. Of the two cases shown in Fig. 4.6, 60℃ case reflects better fuel cell performance in high current region and 60℃ case has higher performance in low current region. In general, PEM fuel cells perform better at higher temperatures for a given RH. However, in this study, the major variable was not the RH of the stream but rather the water flow rate. At a higher temperature, a larger amount of water vapor is required to achieve a given RH condition than the amount required at a lower temperature. For example, at an air temperature of 70℃, to achieve 100% RH 277.3 g_w/kg_{da} of water vapor is required, whereas at an air temperature of 60℃, to achieve 100% RH 152.8 g_w/kg_{da} of water vapor is reequired. Multiplying the air flow rate at 1.2 A/cm^2 (= 64.524 g/min) by those two values, 17.89 g_w/min for 70℃ and 9.86 g_w/min for 60℃ are obtained respectively. The difference is so large that it cannot be overcome by a water injection flow rate of 5 ml/min. Accordingly, for a given water flow rate, the humidification effect is larger when the operating temperature is maintained lower.

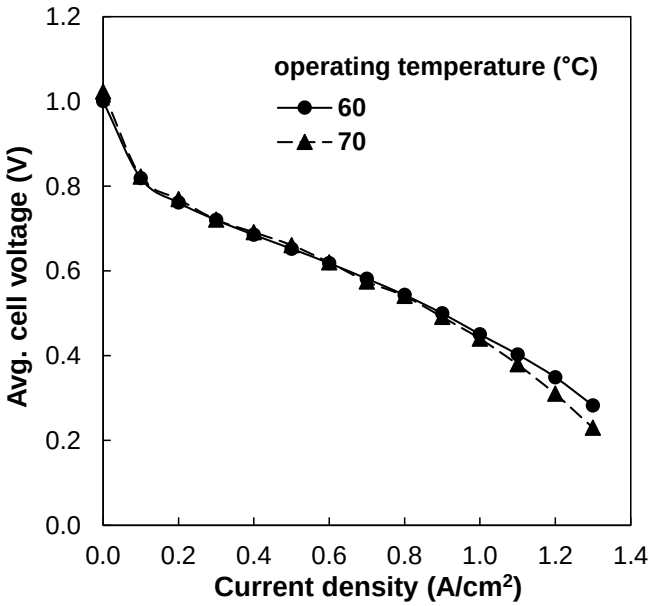

Figure 4.6 Stack performance at operating temperature of 60 and 70℃ when the operating pressure is 1 bar, water injection flow rate is 5 ml/min and injection water temperature is 40℃

4.2.5 Stack operating pressure

Figure 4.7 shows stack performance with different operating pressure when the operating temperature of 60°C, water injection flow rate of 5 ml/min and injection water temperature of 40℃. The trend of this result that stack performance increases with the rise of operating pressure consistent with previous studies. When operating pressure increase the concentration loss decreases. Furthermore, in the pressurized system, stack performance improves because of increase in relative humidity due to the raised partial vapor pressure. It can be recognized from the slope change at the high current density region of this figure.

4.2.6 Cathode stoichiometric ratio

Figure 4.8 shows stack performance with different cathode stoichiometric ratio when the operating temperature of 60°C, operating pressure of 1 bar, water injection flow rate of 5 ml/min and injection water temperature of 40℃. The effect of cathode stoichiometric ratio is not different as already known findings. The stack performance improves with higher cathode SR due to increase of oxygen concentration.

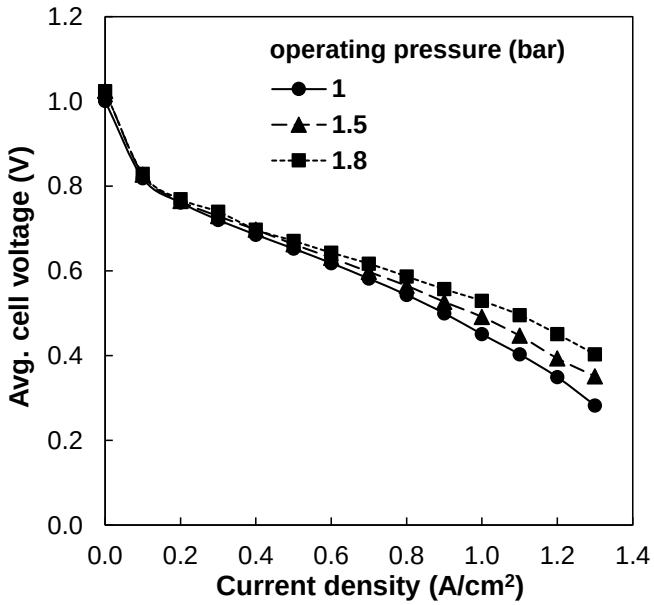

Figure 4.7 Stack performance with different operating pressure when the operating temperature is 60°C, water injection flow rate is 5 ml/min and injection water temperature is 40℃

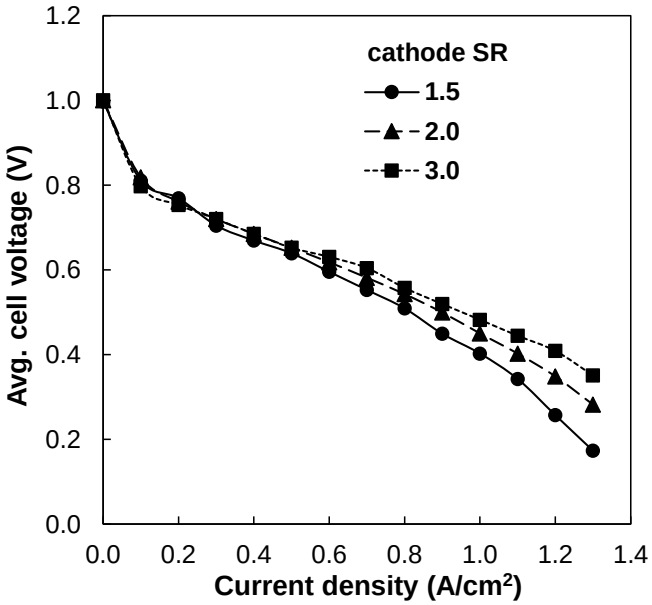

Figure 4.8 Stack performance with different cathode stoichiometric ratio when the operating temperature is 60℃, operating pressure of 1 bar, water injection flow rate is 5 ml/min and injection water temperature is 40℃

4.3 Evaporative cooling performance

4.3.1 Experimental apparatus and test procedure

Experimental setup is the same with Figure 4.1. In the stack performance test using direct water injection method, it should be noted that the water at the cathode flow channel should be removed before every experiment to insure that the effects of water injection are measured accurately. Unlike to stack performance measurement, the water inside the cathode inhibit evaporation of injected water. Hence, purge was progressed until the humidity at the cathode outlet reached a steady state using a large amount of low-humidity air with open circuit voltage (OCV, i.e. without electrical load). And the current was then increased to be within the target high current density region in short time. When the current reached the desired value, it was maintained until the stack performance and dew point temperature of the cathode outlet reached a steady state. Water injection was then begun. While liquid water was being injected into the cathode inlet of the stack, changes in the dew point temperature of the cathode outlet were monitored. And in this part the evaporative cooling performance was investigated at high current region because this region generate much heat and required additional cooling

capacity.

In measurement of the evaporative cooling performance, dew point temperature of the cathode outlet is key value and it takes long time to reach a steady state due to its slow response. Hence, it took a long time more than 30 minutes to obtain the exact value.

4.3.2 Water injection flow rate and stack operating temperature

Figure 4.9 shows the evaporative heat rejection rate at operating temperatures of 60 and 70℃ for various water injection flow rates and high current densities. The evaporative heat rejection rate is calculated using Eqs. (4.1) and (4.2).

$$Q_{\text{evap}} = \dot{m}_{\text{evap}} \cdot \Delta h \tag{4.1}$$

$$\Delta h = h_{\text{vapor, out}} - h_{\text{water, in}} \tag{4.2}$$

In Eq. (4.2), $h_{\text{water, in}}$ is the enthalpy of the liquid water at the water injection temperature, and $h_{\text{vapor, out}}$ is the enthalpy of the water vapor at the temperature of the cathode outlet. By measuring the temperature of injected water and the cathode outlet air the enthalpy values can be obtained from the US National Institute of Standards' REFPROP database (NIST, USA). In Fig.

4.9, the evaporative heat rejection rate increases with an increase in the water flow rate. This is mainly due to the effect that the larger amount of water injection lead to the increase of the evaporation rate. Figure 4.10 shows the evaporation efficiency at operating temperatures of 60 and 70℃ for various water injection flow rates and high current densities. The evaporation efficiency is defined as the mass ratio of the evaporated water to the injected water, expressed as a percentage. Of the two cases shown in Fig. 4.9, case (b) reflects a greater evaporation efficiency than case (a). This means that at a higher operating temperature, a larger amount of water evaporates and the enthalpy difference increases. The effect of temperature on the evaporation efficiency can also be observed in Fig. 4.10. In terms of the evaporative heat rejection rate, the system cannot provide all of the cooling capacity by using coolant (deionized water in this study). At the operating temperature of 70°, the current density of 1.2 A/cm^2 and the water injection flow rate of 5 ml/min, the evaporative heat rejection rate was about 68 W in Fig. 4.9. Which was only 7.6% of the heat rejection rate by the coolant at 1000s of Fig. 3.9, about 890 W. However, it does provide additional cooling capacity so reduces heat rejection load in existing coolant radiator. Besides it offers advantages that do not require any design changes to the stack or existing cooling system.

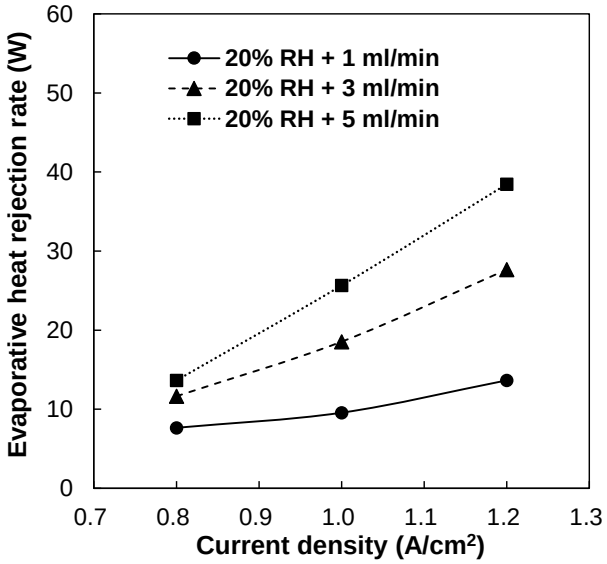

(a) 60℃

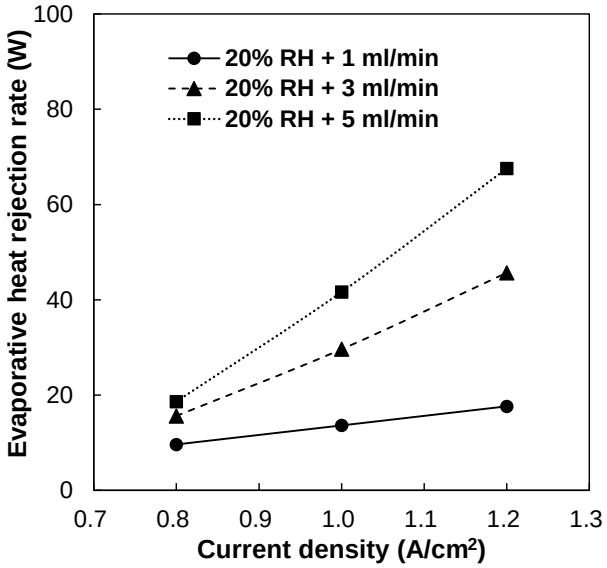

(b) 70℃

Figure 4.9 Evaporative heat rejection rate for a given operating temperature for various water injection flow rates at high current densities

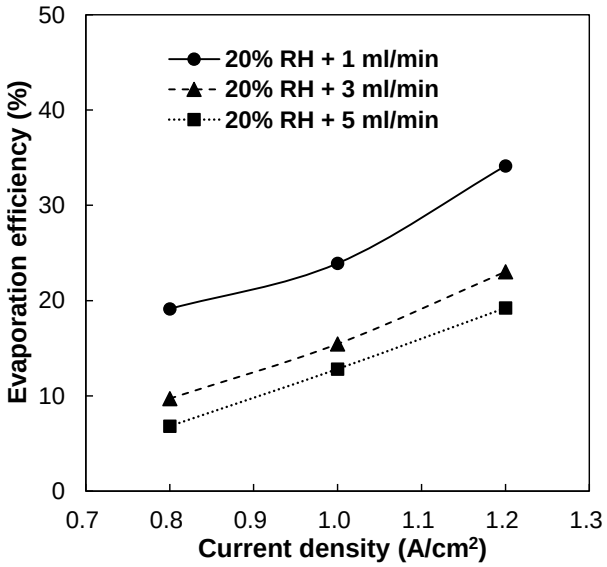

(a) 60℃

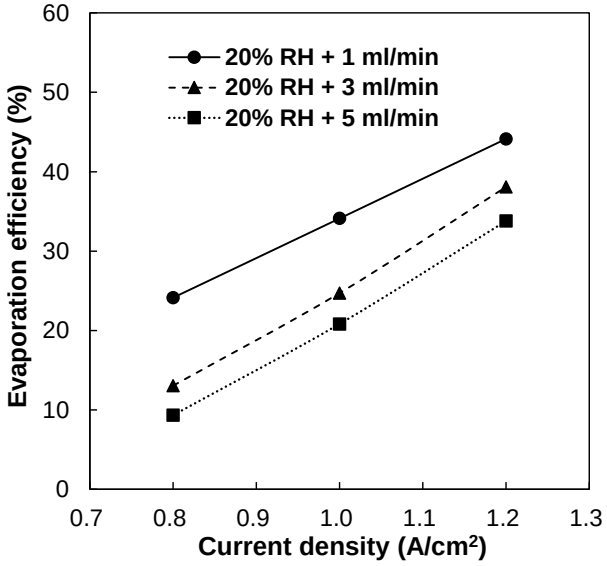

(b) 70℃

Figure 4.10 Evaporation efficiency for a given operating temperature for various water injection flow rates at high current densities when the operating pressure is 1 bar and injection water temperature is 40℃

4.3.3 Injection water temperature

Figure 4.11 shows dew point temperature at the cathode outlet with different injection water temperatures when the operating temperature of 60℃, operating pressure of 1 bar and water injection flow rate of 5 ml/min. Overall, the dew point temperature at the cathode outlet increases with the rise of the injection water temperature. The dew point temperature at the cathode outlet means water vapor per unit mass of dry air in the same operating pressure. And because the cathode SR is fixed, water vapor released at the cathode outlet is proportional to dew point temperature when the current density is the same. Accordingly it means evaporative heat rejection rate increases with the rise of the injection water temperature. This trend reflects the simulation result of the chapter 2. This is due to facilitated heat and mass transfer at water droplet surface in higher temperature.

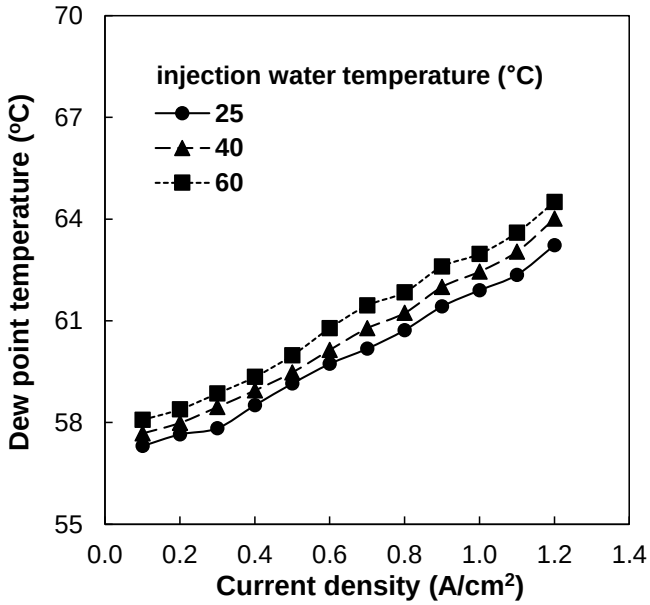

Figure 4.11 Dew point temperature at the cathode outlet with different injection water temperatures when the operating temperature is 60℃, operating pressure is 1 bar and water injection flow rate is 5 ml/min

4.3.4 Stack operating pressure

Figure 4.12 shows dew point temperature at the cathode outlet with different stack operating pressure when the operating temperature of 60℃, water injection flow rate of 5 ml/min and injection water temperature of 40℃. Unlike to the effect of injection water temperature, dew point temperature is directly connected to vapor release at the cathode outlet in these case. Because the operating pressure is different each other. Humidity ratio, mass of water vapor per unit mass of dry air (g_w/kg_{da}), is affected by the pressure (not only the partial vapor pressure but also the total gas pressure). And when the total gas pressure increases the humidity ratio decreases by Eq. (3.3). Furthermore, as shown in Figure 4.13, the dew point temperature at the cathode outlet decreases with the increase of operating pressure. Because in pressurized condition the partial vapor pressure increases proportional to the total gas pressure which means the same vapor pressure is obtained with smaller amount of water vapor. As a result, when the operating pressure increases the evaporation of injected water is reduced and evaporative cooling capacity is also do.

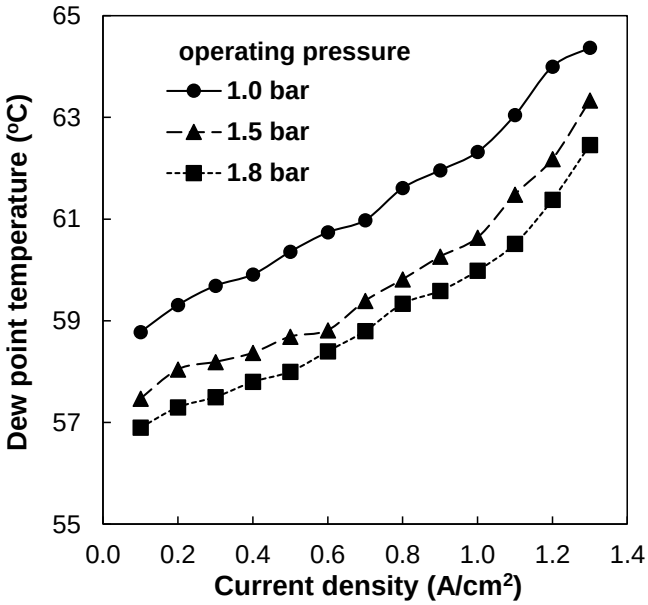

Figure 4.12 Dew point temperature at the cathode outlet with different stack operating pressure when the operating temperature is 60℃, water injection flow rate is 5 ml/min and injection water temperature is 40℃

4.3.5 Cathode stoichiometric ratio

Figure 4.13 shows dew point temperature at the cathode outlet with different cathode stoichiometric ratio when the operating temperature is 60℃, operating pressure is 1 bar and injection water temperature is 40℃. In the case of SR change, the vapor flow rate at the cathode outlet is not simply inferred by dew point temperature. Because the water vapor flow rate is determined by the product of humidity ratio and dry air flow rate which is affected by SR number. Hence, the vapor release at the cathode outlet is calculated and shown in the Figure 4.14. From this figure it can be found that the vapor release at the cathode outlet increase with higher SR number but the curves are converging with rise of current density. This is because the water injection flow rate is constant which means that the maximum amount of water evaporation has limit value. Calculation of the relative evaporative heat rejection rate from the vapor release at the cathode outlet is shown in Figure 4.15. As shown in this figure, the maximum value was recorded when the difference between the SR numbers the greater.

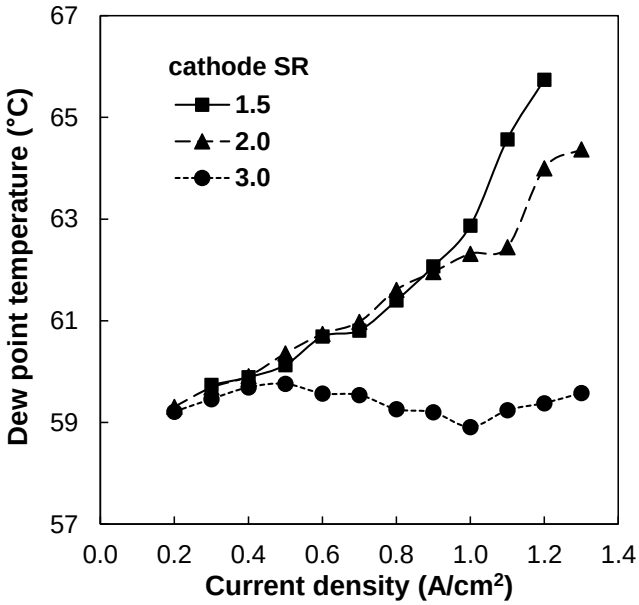

Figure 4.13 Dew point temperature at the cathode outlet with different cathode stoichiometric ratio when the operating temperature is 60℃, operating pressure is 1 bar and injection water temperature is 40℃

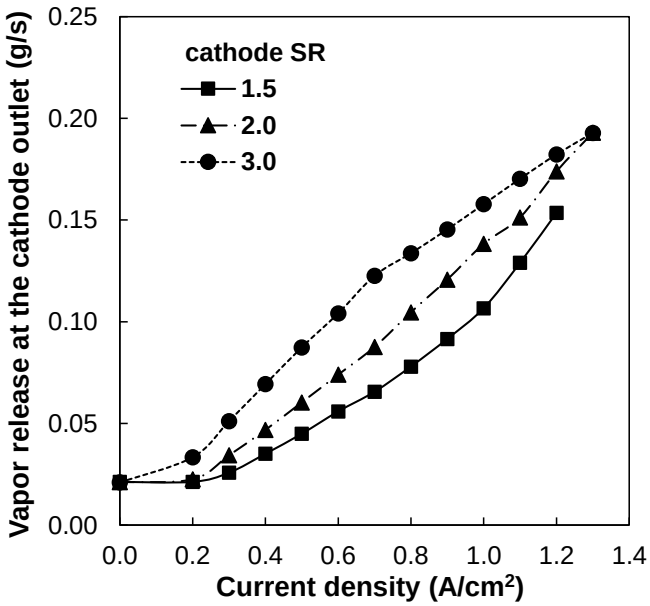

Figure 4.14 Vapor release at the cathode outlet with different cathode stoichiometric ratio

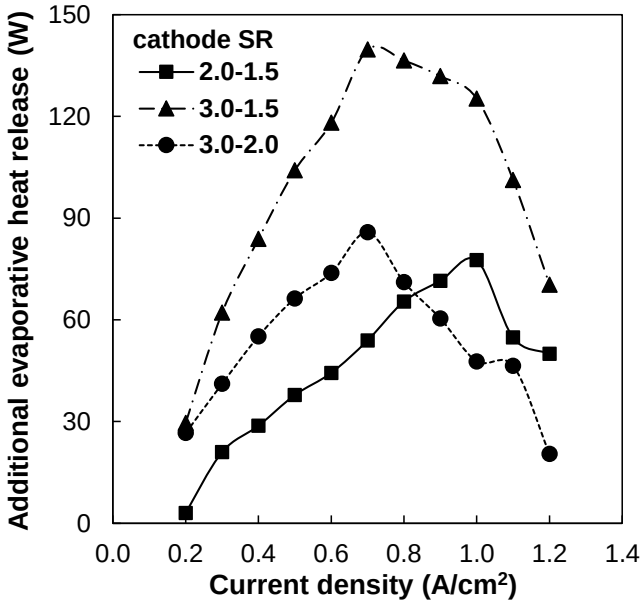

Figure 4.15 Additional evaporative heat release with different cathode stoichiometric ratio

4.4 Development of an operating strategy for PEMFCs with a direct water injection system and verification

4.4.1 The effects of intermittent water injection

From the previous chapter, the necessity for proper adjustment of water injection were raised. The objective in this chapter is to develop a strategy to control water injection while preventing flooding and water shortages. Evaporative cooling performance will also be considered as well as humidification performance. To achieve this goal intermittent water injection will be applied as a strategy. And the effect of direct water injection method for start-up characteristic was also investigated experimentally.

Figure 4.16 shows schematic diagram of water injection strategy. As shown in this figure water is not injected continuously. Instead, inject water with interval and the injection flow rate is adjusted considering target relative humidity and operating temperature.

$$\dot{m}_{v,req} = \frac{M_v}{M_a}\left(\frac{\phi_t P_s}{P-\phi_t P_s} - \frac{\phi_{in} P_s}{P-\phi_{in} P_s}\right)\dot{m}_{a,in} \tag{4.3}$$

In Eq. (4.3) $\dot{m}_{v,req}$ is water injection mass flow rate to achieve target relative humidity assuming all the injected water evaporate to vapor phase. In

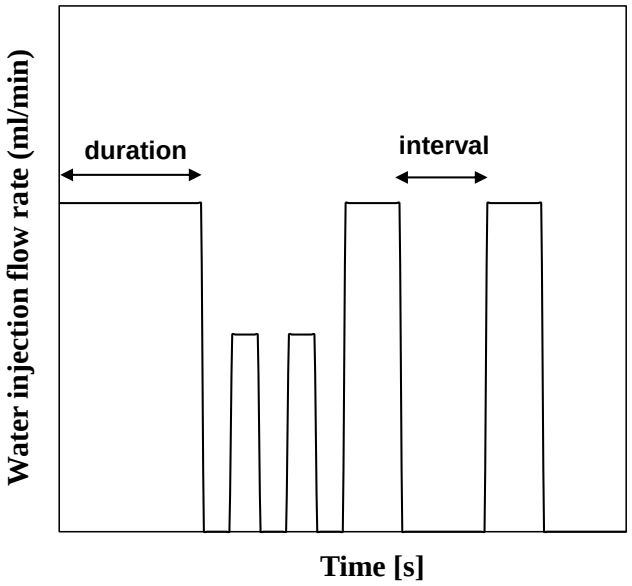

Figure 4.16 Schematic diagram of water injection strategy

this equation, to determine water injection flow rate relative humidity of inlet air (dry air), target relative humidity, operating temperatures and current density are considered. And the injection duration/interval are set by stack operating conditions. Through this time change strategy the stack performance can be obtained stably without flooding.

Figure 4.17 shows required water vapor flow rate, calculation of Eq. (2.3). In this figure, when the operating temperature and the target relative humidity is high, the required water vapor flow rate increases. This value can be more than water production rate of fuel cell stack at the high current density region so continuous injection may cause lack of water to inject.

Figure 4.18 shows stack performance with different target relative humidity at the cathode inlet when continuous injection is applied. The experiments with the concept of target relative humidity were conducted through the new PEMFC stack with active area of 300 cm^2. So its performances may differ from the results with the existing stack with active area of 250 cm^2. In this figure, the best performance is when the target relative humidity is 100%. The performance of the 125% target relative humidity is even lower to that of the 75% target relative humidity. This difference increases with the rise of the current density. It is because of the worsening of water disproportion in the fuel cell due to flooding phenomena.

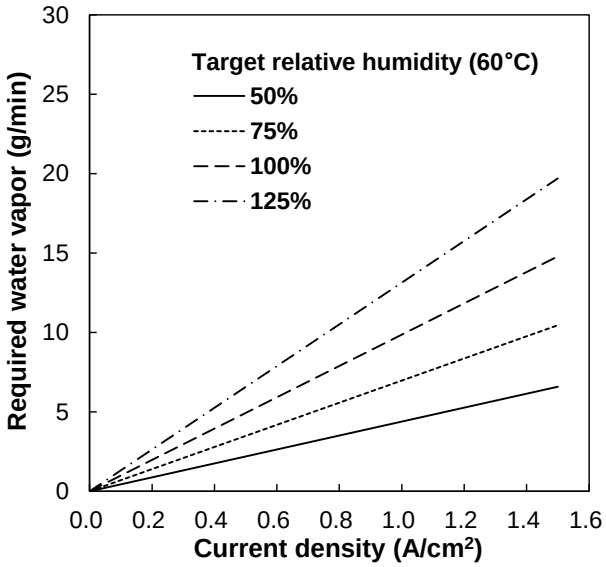

(a) for various target relative humidity at the operating temperature of 60℃

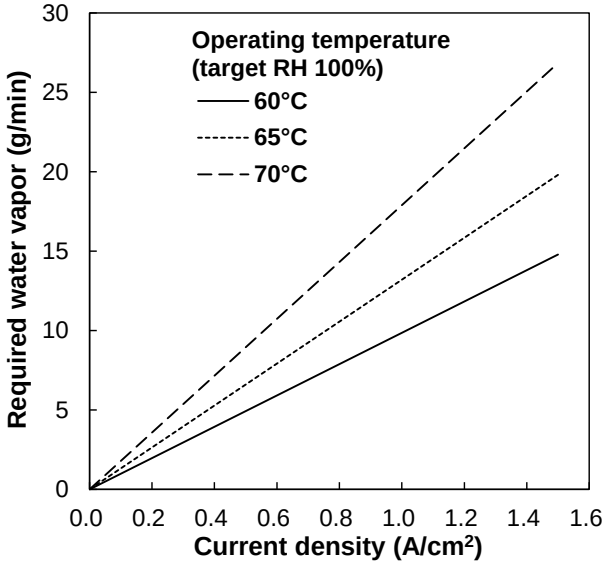

(b) for various operating temperature at the 100% target relative humidity

Figure 4.17 Required water vapor flow rate

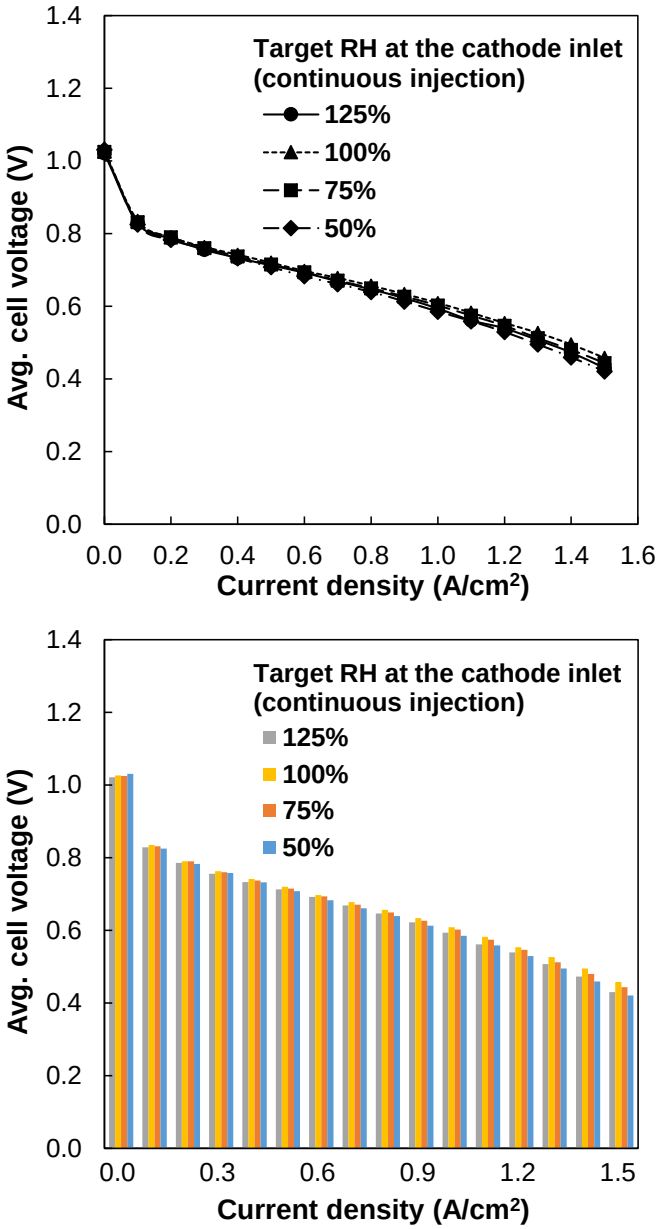

Figure 4.18 Stack performance with different target relative humidity at the cathode inlet (continuous injection)

Figure 4.19 shows stack performance with different injection strategies at the 50% target relative humidity at the cathode inlet. In this figure, the best performance is when the continuous injection is applied. From this result, intermittent injection is not effective when the water injection flow rate is too low. Furthermore, even in high current density region which produce a lot of water humidification is required.

Figure 4.20 shows stack performance with different injection strategies at the 100% target relative humidity at the cathode inlet. In this figure, the best performance is when the intermittent water injection strategy of injection 5s, interval 5s is applied. When the water injection timing is 3s, the performance is low because the humidification is insufficient. On the other hand, when the water injection timing is 7s, the flooding phenomenon occurred in the high current density region. From this figure, intermittent water injection strategy which relieve flooding in the cathode channel by injection and interval timing control was verified to be effective.

Figure 4.21 shows comparison of stack performance with/without water injection and injection strategies. The performance with the relative humidity of 50, 100% by gas humidification of bubbler humidifier are presented as standards. The performance with the relative humidity of 100% is the best performance we may attain. The performance with the relative humidity of

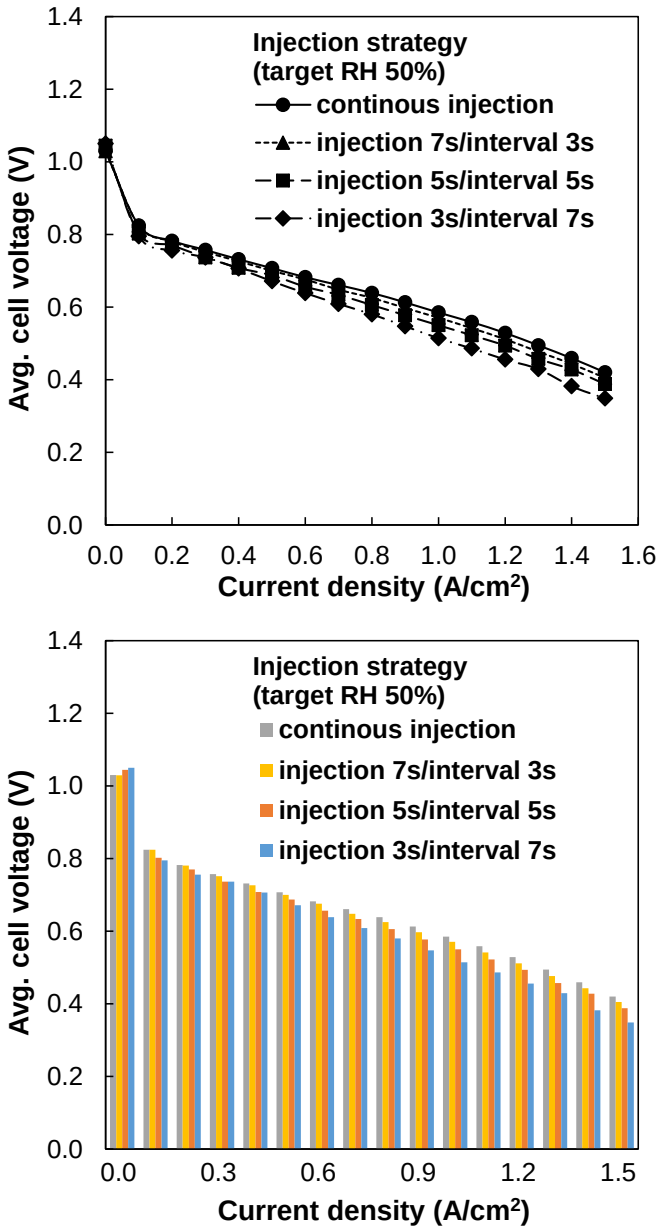

Figure 4.19 Stack performance with different injection strategies at the 50% target relative humidity at the cathode inlet

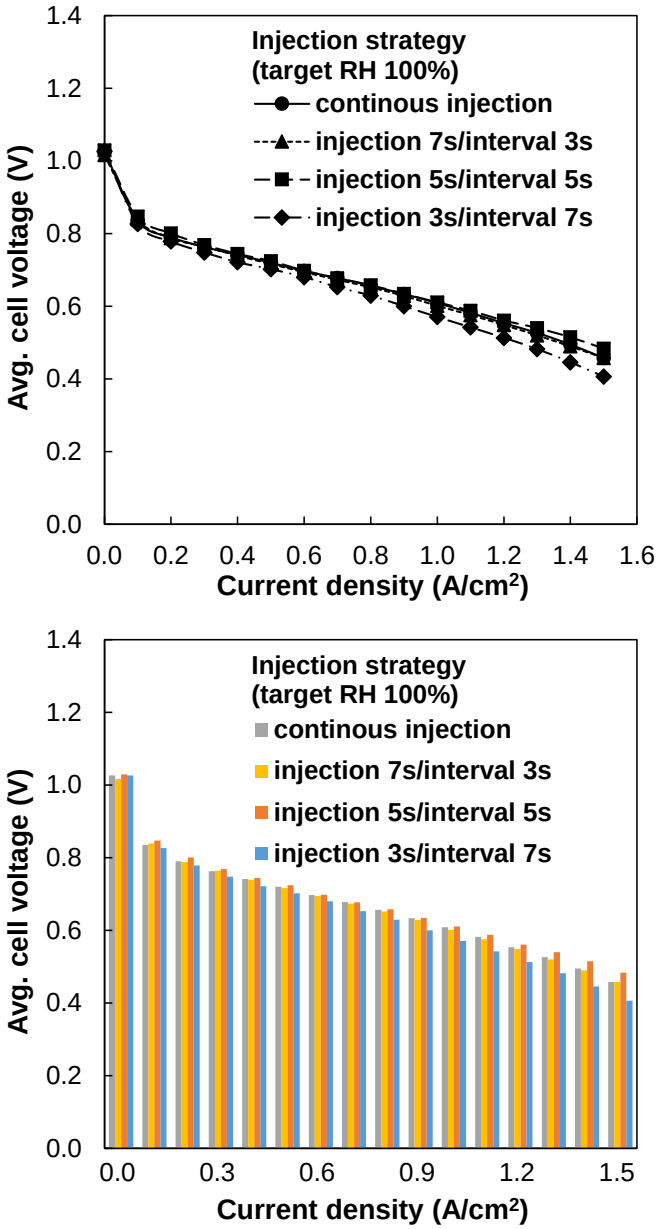

Figure 4.20 Stack performance with different injection strategies at the 100% target relative humidity at the cathode inlet

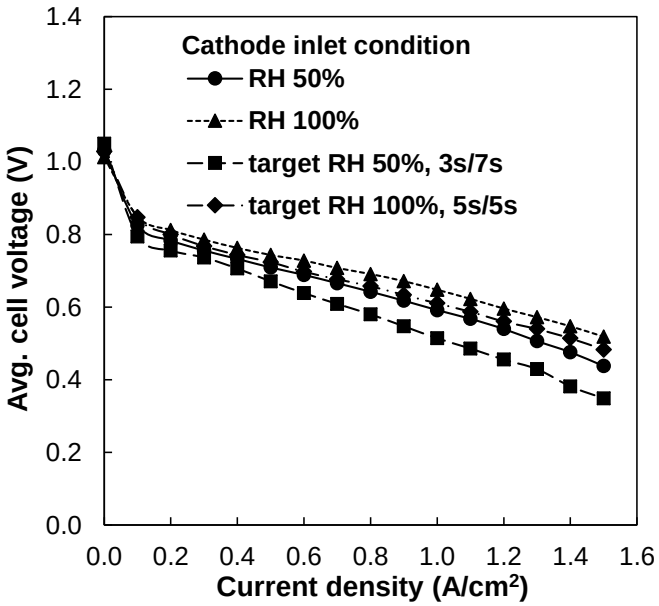

Figure 4.21 Comparison of stack performance with/without water injection and injection strategies

50% is the performance as known the limiting performance in the automotive PEMFC systems at the high current density region. In figure 4.21, the best performance with intermittent water injection strategies is when the target relative humidity is 100% and injection/internal timing is 5s. This performance is comparable to that of the relative humidity is 70%.

Figure 4.22 shows the result which is applied such injection strategy at high current density of 1.0 A/cm^2. As shown in this figure, the stack performance and dew point temperature of the cathode outlet increase immediately and the values are maintained stably at injection condition.

Figure 4.23 shows the dew point temperature of the cathode outlet with continuous and intermittent injection when the operating temperature is 60℃, operating pressure is 5 ml/min and injection water temperature is 40℃. As shown in this figure the dew point temperature of the cathode outlet is higher when the intermittent injection strategy is applied. Considering injection duration and interval time of intermittent water injection strategy, the injection flow rate is the same as 5 ml/min. In this case, the higher dew point temperature means more evaporation of injected water and larger evaporation efficiency. The reason is that the intermittent water injection strategy provide additional time for evaporation to the water inside the cathode.

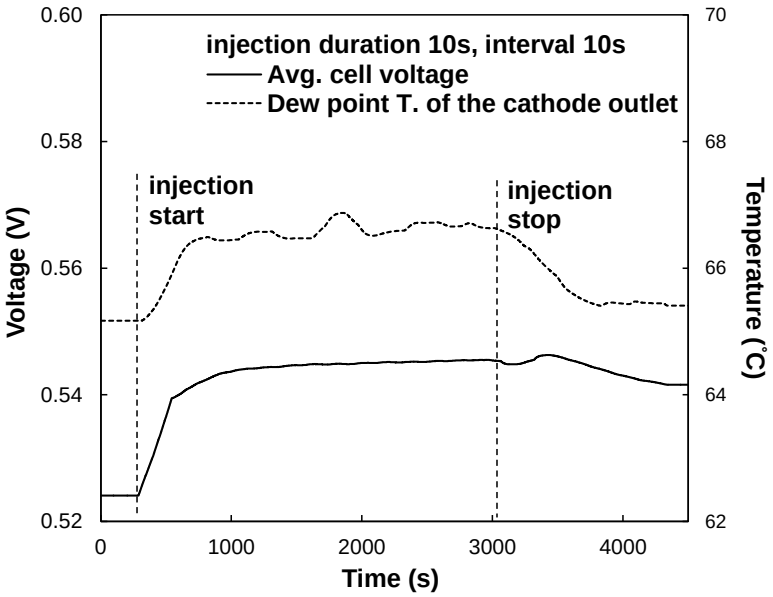

Figure 4.22 Changes in average cell voltage and dew point temperature at the cathode outlet at an operating temperature of 60℃, current density of 1.0 A/cm^2 with a water injection strategy

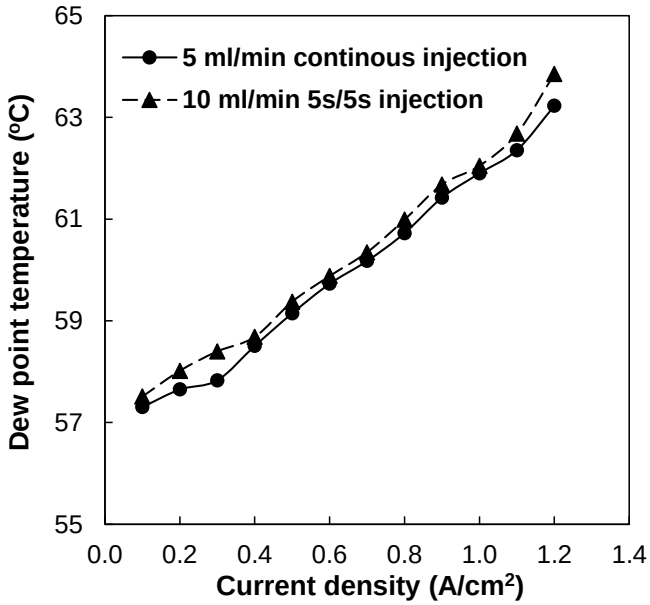

Figure 4.23 Dew point temperature at the cathode outlet with continuous and intermittent injection when the operating temperature is 60℃, operating pressure is 5 ml/min and injection water temperature is 40℃

4.4.2 Start-up with a direct water injection system

Start-up with the direct water injection system is also investigated experimentally. Figure 4.24 shows the effect of water injection on the stack performance after start-up at a constant voltage. At temperature of 25°C and constant voltage of 0.4 V, the current sharply increases after start-up and dropped soon. Because the stack temperature is low which is insufficient for water evaporation the load does not increase. This result represents that it is hard to evaporate for injected water at a too low temperature. Therefore, to get the benefits of humidification by water injection the fuel cell stack should be warmed up to certain temperature first. At temperature of 45°C and constant voltage of 0.6 V, the current sharply increases after start-up and the current is maintained. The current of start-up with water injection is higher than that with not humidified dry air. Besides, in the case with 3ml/min, the current increases gradually which means the stack performance is improving slowly.

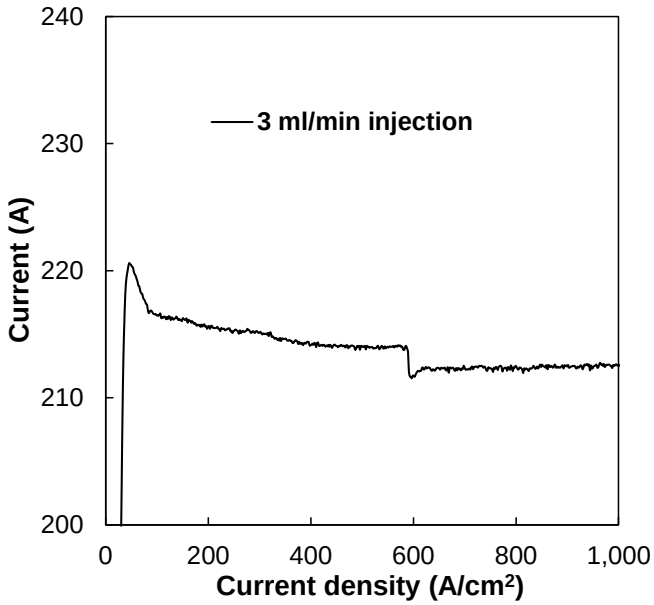

(a) 25℃ at constant voltage of 0.4 V

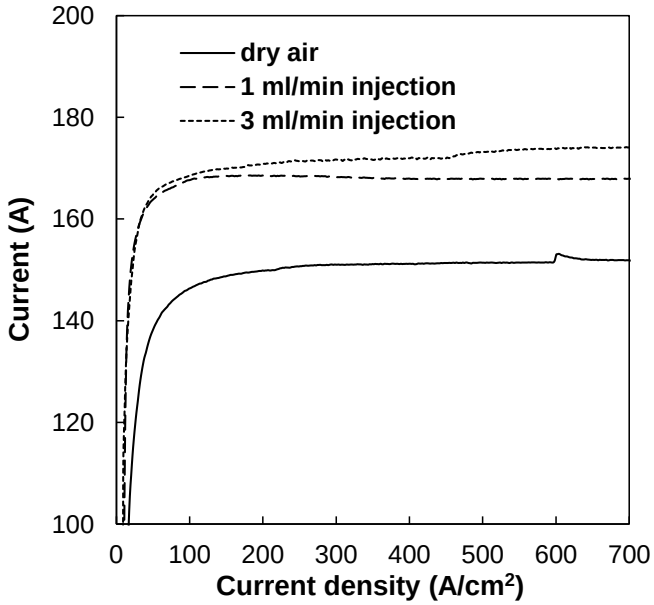

(b) 45℃ at constant voltage of 0.6 V

Figure 4.24 The effect of water injection on the stack performance after start-up at a constant voltage

4.5 Summary

In this chapter, the operating characteristics of PEM fuel cells with a direct water injection system were investigated to provide useful information and better understanding on this system. Water injection flow rate, water injection temperature, stack operating temperature, stack operating pressure and cathode stoichiometric ratio are considered as operating variables. The humidification performance was enhanced when water injection flow rate, water injection temperature, stack operating pressure is higher and stack operating temperature is lower. But, water flow rate should be properly adjusted in order to prevent flooding at high current region. The evaporative cooling performance was enhanced when water injection flow rate, water injection temperature, stack operating temperature, stoichiometric ratio is higher and stack operating pressure is lower.

Chapter 5. Concluding remarks

In this study, to eliminate the need for a bulky humidifier and to lighten the cooling load of PEM fuel cells, a simultaneous cathode humidification and evaporative cooling system using an external-mixing air-assist atomizer was developed, and its performance was investigated both numerically and experimentally.

(1) Measurement of the atomization performance indicated that the air-assist nozzle produced very fine droplets, 20 to 25 μm in diameter, at a pressure difference of 50 kPa and the given air-to-liquid ratios. And due to its small variation of droplet diameter, the effect of droplet size on the humidification and evaporative cooling is not considered in this study.

(2) The results of the stack performance experiments show that the direct water injection method proposed in this paper is quite effective in cathode humidification. This system takes only a small volume and able to humidify in an active manner unlike to other passive humidifiers such as membrane humidifier. The stack performance improved with an increased water flow rate because of the increased humidification effect. At a given water flow rate, the improvement in the stack performance that can be attributed to the humidification effect was greater when the operating temperature was lower.

(3) The water injection method also have advantage in the cooling of

PEM fuel cells at high current densities. Although this method is not sufficient to substitute existing cooling system, it provides additional cooling capacity so reduces heat rejection load in existing coolant radiator. The evaporation rate was larger at a higher operating temperature and higher water injection flow rate. The evaporation efficiency was larger at higher mass ratio between cathode inlet air and injected water.

(4) The best stack performance was achieved when the operating temperature was 60℃ and the water injection flow rate was 5 ml/min. The stack performance under this condition was superior to that when the relative humidity of the air at the cathode inlet was 60%. The maximum evaporative heat rejection rate was achieved when the operating temperature was 70℃, the water injection flow rate was 5 ml/min, and the current density was 1.2 A/cm^2.

(5) More stable operation and larger evaporation efficiency was achieved by applying intermittent water injection strategy. The danger of flooding decreased and the evaporative cooling performance improved with the intermittent water injection. Moreover, in start-up process water injection method had advantage that it can humidify inside the cathode actively.

In brief, the humidification effect was equal or superior to that when the cathode inlet air was 50% RH. And it have advantages in terms of system

volume and active control. The evaporative cooling effect was insufficient to manage all the heat generation from the stack, but it provided considerable additional cooling capacity. Therefore, the direct water injection method can be a useful technology for PEM fuel cell systems. In automotive PEMFC systems in particular, in which space is limited, this method can offer considerable advantages.

References

[1] Jian Q, Ma G, Qiu X. Influences of gas relative humidity on the temperature of membrane in PEMFC with interdigitated flow field. Renewable Energy. 2014;62:129-36.

[2] Ramya K, Sreenivas J, Dhathathreyan KS. Study of a porous membrane humidification method in polymer electrolyte fuel cells. Int. J. Hydrogen Energy 2011;36(22):14866–72.

[3] Wan ZM, Wan JH, Liu J, Tu ZK, Pan M, Liu ZC, et al. Water recovery and air humidification by condensing the moisture in the outlet gas of a proton exchange membrane fuel cell stack. Appl. Therm. Eng. 2012;42:173–8.

[4] Kong IM, Choi JW, Kim SI, Lee ES, Kim MS. Experimental study on the self-humidification effect in proton exchange membrane fuel cells containing double gas diffusion backing layer. Appl. Energy 2015;145:345-53.

[5] Kim BJ, Kim MS. Studies on the cathode humidification by exhaust gas recirculation for PEM fuel cell. Int. J. Hydrogen Energy 2012;37(5):4290-4299.

[6] Zhang G, Kandlikar SG. A critical review of cooling techniques in proton exchange membrane fuel cell stacks. Int. J. Hydrogen Energy 2012;37(3):2412-29.

[7] Kandlikar SG, Lu Z. Thermal management issues in a PEMFC stack – A brief review of current status. Appl. Therm. Eng. 2009;29(7):1276-80.

[8] Pei P, Chen H. Main factors affecting the lifetime of Proton Exchange Membrane fuel cells in vehicle applications: A review. Appl. Energy 2014;125:60-75.

[9] Hosseinzadeh E, Rokni M, Rabbani A, Mortensen HH. Thermal and water management of low temperature Proton Exchange Membrane Fuel Cell in fork-lift truck power system. Appl. Energy 2013;104:434-44.

[10] Dadda B, Abboudi S, Zarrit R, Ghezal A. Heat and mass transfer influence on potential variation in a PEMFC membrane. Int. J. Hydrogen Energy 2014;39(27): 15238–45.

[11] Chandan A, Hattenberger M, El-kharouf A, Du S, Dhir A, Self V, et al. High temperature (HT) polymer electrolyte membrane fuel cells (PEMFC) - A review. J. Power Sources 2013;231(1):264-78.

[12] Rogg S, Hoglinger M, Zwittig E, Pfender C, Kaiser W, Heckenberger T. Cooling modules for vehicles with a fuel cell drive. Fuel Cells 2003;3(3):153-8.

[13] Ahluwalia RK, Wang X. Fuel cell systems for transportation:status and trends. J. Power Sources 2008;177(1):167-76.

[14] Ahluwalia RK, Wang X, Kwon J, Rousseau A, Kalinoski J, James B, et al. Performance and cost of automotive fuel cell systems with ultra-low platinum loadings. J. Power Sources 2011;196(10):4619-30.

[15] Wang Y, Chen KS, Mishler J, Cho SC, Adroher XC. A review of polymer electrolyte membrane fuel cells: technology, applications, and needs on fundamental research. Appl. Energy 2011;88(4):981–1007.

[16] Berger O, Schmitz S, Görner K. Optimization of a fuel-cellcooling-system for automotive transportation at Volkswagen. 2008 Fuel Cell Seminar & Exposition; 2008.

[17] Kim H, Joo K, Won S, Han K, Lee J. A detailed study of fuel cell vehicle cooling system. 2012 JSAE Annual Congress; 2012.

[18] Wang J, Shi M. Study on two-phase countercurrent flow and transport phenomenon in PEM of a direct methanol fuel cell. Sci. China Ser. E 2006;49(1):102–14.

[19] Nam JH, Kaviany M. Effective diffusivity and water-saturation distribution in single- and two-layer PEMFC diffusion medium. Int. J. Heat Mass Tran. 2003;46(24):4595–611.

[20] Wood DL, Yi JS, Nguyen TV. Effect of direct liquid water injection and interdigitated flow field on the performance of proton exchange membrane fuel cells. Electrochim. Acta 1998;43(24):3795-809.

[21] Perry ML, Meyers JP, Darling RM, Evans C, Balliet R. Evaporatively-cooled PEM fuel-cell stack and system. ECS Transactions 2006;3(1):1207-14.

[22] Reiser C. Ion exchange membrane fuel cell power plant with water management pressure differentials. US Patent 5700595; 1997.

[23] Weber AZ, Darling RM. Understanding porous watertransport plates in polymer-electrolyte fuel cells. J. Power Sources 2007;168(1):191-9.

[24] Darling R, Meyers J, Balliet R. Non-circulating coolant PEM fuel cell power plant assembly with low thermal mass. US Patent 7638217; 2009.

[25] Darling RM, Perry ML. Evaporatively cooled hybrid PEM fuel cell power plant assembly. US Patent 7887966; 2011.

[26] Reiser CA, Meyers JP, Johnson DD, Evans CE, Darling RM, Skiba T, Balliet RJ. Fuel cells evaporative reactant gas cooling and operational freeze prevention. US Patent 7579098; 2009.

[27] Goebel SG. Evaporative cooled fuel cell. US Patent 6960404; 2005.

[28] Brambilla M, Mazzucchelli G. Fuel cell with cooling system based on direct injection of liquid water. US Patent 6835477; 2004.

[29] Jung SH, Kim SL, Kim MS, Park YS, Lim TW. Experimental study of gas humidification with injectors for automotive PEM fuel cell systems. J. Power Sources 2007;170(2):324-33.

[30] Hede PD, Bach P, Jensen AD. Two-fluid spray atomisation and pneumatic nozzles for fluid bed coating/agglomeration purposes: A review. Chem. Eng. Sci. 2008;63(14):3821-42.

[31] Walzel P. Liquid atomisation. Int. Chem. Eng. 1993;33(1):46-60.

[32] Spraying Systems Co. AIR ATOMIZING & AUTOMATIC SPRAY NOZZLES, http://www.spray.com/cat75/automatic-m/offline/download.pdf; 2013.

[33] Lefebvre AH. Atomization and Sprays. Hemisphere Pub. Corp., ISBN 0891166033; 1989.

[34] McQuiston FC. Heating, ventilating, and air conditioning: analysis and design. John Wiley & Sons, ISBN 0471470155; 2005.

[35] Wagner W, Pruß A. The IAPWS formulation 1995 for the thermodynamic properties of ordinary water substance for general and scientific use. J. Phys. Chem. Ref. Data 2002;31(2):387-535.

[36] Mehmood A, An M, Ha HY. Physical degradation of cathode catalyst layer: A major contributor to accelerated water flooding in long-term operation of DMFCs. Appl. Energy 2014;129:346-53.

[37] Kim SI, Baik KD, Kim BJ, Lee NW, Kim MS. Experimental study on mitigating the cathode flooding at low temperature by adding hydrogen to the cathode reactant gas in PEM fuel cell. Int. J. Hydrogen Energy 2013;38(3):1544-52.

[38] Kim SL, Studies on the humidification for automotive PEM fuel cell systems using injectors, MS diss., Seoul National University, 2007.

[38] Song JH, Studies on the internal humidification with water absorbing sponge for automotive PEM fuel cell systems, MS diss., Seoul National University, 2007.

국 문 초 록

일반적으로 고체의 이온전도도는 액체에 비해 극히 작지만, 고분자 전해질막 연료전지에 사용되는 고분자 전해질막은 술폰화(sulfonation)에 의해 막이 습윤 상태에 있을 때, 양성자가 물분자와 결합된 상태로 원활히 이동하게 된다. 따라서 고분자 막의 수화도는 연료전지의 성능을 결정짓는 중요한 요소이며, 이를 높게 유지하기 위해 가습이 필수적이다. 하지만 기존의 고분자 전해질막 연료전지 시스템에 사용된 가습기는 부피가 매우 크고 무거워 시스템을 복잡하게 하고, 많은 제작 비용이 소모된다. 또한 능동적인 습도 조절이 어렵고 동력 손실이 발생할 수도 있다는 단점이 있다. 가습과 마찬가지로, 고분자 전해질막 연료전지의 열방출은 성능과 내구성에 매우 큰 영향을 미친다. 고분자 전해질막 연료전지가 매우 높은 에너지 변환 효율을 갖지만 고출력 운전구간에서는 전기출력에 버금가는 폐열이 발생하기 때문이다. 게다가 고온에서는 전해질막과 촉매층의 열화가 촉진되어 장기적으로 스택 내구성을 낮출 수 있다. 따라서 스택의 과열을 막고 60°C~80°C 의 적정 운전온도를 유지하기 위해서는 생성되는 열을 효과적으로 제거할 필요가 있다. 연료전지 냉각을 위한 여러 가지 방안이 제시되어 있지만 충분한 냉각 용량을 확보하기 위해서는 넓은 열전달 면적을 가진 방열기를 사용하는 것 외에 특별한 대안이 없는 상황이다. 하지만 자동차와 같이 시스템을 위한 공간에 제약이 있을 경우 방열기의 크기는 제한될 수 밖에 없으며 냉각용량 역시 제한된다. 이처럼 방열기에서 충분한 냉각 용량을 확보하지 못할 경우 스택의 과열을 막기 위해서는 출력을 제한할 수 밖에 없다. 이 같은 현 상황에서 기존의 가습 및 냉각 방식을 대체 혹은 보조할 수 있는 새로운 시스템의 개발은 매우 시급하고 절실하다고 할 수 있다. 본 연구에서는 이러한 가습 및 열방출 문제에 대한 해결책의 하나로 물 직접분사를 이용한 고분자

전해질막 연료전지의 가습 및 증발냉각에 관한 연구를 수행하였다. 이를 위하여, 먼저 물 직접분사 방식을 적용한 연료전지에서 운전조건에 따른 채널 내부 액적의 증발특성과 그것이 성능에 미치는 영향에 관하여 해석적 연구를 수행하였다. 그 결과 분사된 물의 증발에 의한 내부 기체의 상대습도 상승과 증발냉각 효과를 확인하였다. 그 후, 공기보조식 미립화 노즐을 사용한 물 직접분사 시스템을 개발하고 이를 탑재한 실험장치를 제작하여 기초실험을 수행하였다. 실험결과 공기극 입구에서 물을 분사하는 즉시 스택의 성능이 상승하는 것을 확인할 수 있었고 공기극 후단의 노점을 측정함으로써 분사된 물이 증발하며 냉각효과를 발휘한다는 사실 또한 확인하였다. 기초실험을 수행한 후에는 다양한 운전조건에서 각각의 변수들이 미치는 영향을 알아보기 위해 물 분사량, 물 분사온도, 스택 운전온도, 공기유량, 운전압력에 관련된 실험을 통하여 운전특성을 파악하였다. 마지막으로 앞서 파악한 운전특성을 고려하여 내부 수분 균형, 간헐적 분사, 초기시동 특성에 관련된 운전전략을 세우고 이를 검증함으로써 물 직접분사 방식의 적용 가능성을 살펴보았다. 그 결과 기존 가습기 대비 작은 부피로도 동등하거나 더 우수한 가습 성능을 달성할 수 있었으며 추가적으로 증발냉각 효과로 인해 스택 열관리 측면에서의 장점도 확인할 수 있었다. 본 연구의 결과를 종합해 봤을 때 고분자 전해질막 연료전지의 가습과 냉각에 물 직접분사 방식을 충분히 적용할 수 있을 것으로 기대된다. 특히 가습기의 부피를 줄일 수 있게 됨으로써 시스템 소형화에 기여할 수 있고 고출력 운전구간에서 추가적인 냉각용량을 확보 함으로써 장기적으로 스택 내구성 향상에 도움이 될 것으로 기대된다.

주요어: 고분자 전해질막 연료전지, 공기극 가습, 증발냉각, 물 직접분사, 공기보조식 미립화 노즐

학 번: 2009-23918